

# Quantifying Post-Fire Aeolian Sediment Transport Using Rare Earth Element Tracers

---

A Thesis  
Submitted to the  
Temple University Graduate Board

---

In Partial Fulfillment  
Of the Requirement for the Degree  
MASTER OF SCIENCE  
GEOLOGY

---

by  
David A. Dukes  
May 2017

---

Dr. Sujith Ravi, Thesis Advisor

---

Dr. David E. Grandstaff

---

Dr. Ilya V. Buynevich

## ABSTRACT

Grasslands provide fundamental ecosystem services in many arid and semi-arid regions of the world, but are experiencing rapid increases in fire activity making them highly susceptible to post-fire accelerated soil erosion by wind. A quantitative assessment that integrates fire-wind erosion feedbacks is therefore needed to account for vegetation change, soil biogeochemical cycling, air quality, and landscape evolution. We investigated the applicability of a novel tracer technique – the use of multiple rare earth elements (REE) - to quantify aeolian soil erosion and to identify sources and sinks of wind-blown sediments in a burned and unburned shrub-grass transition zone in the Chihuahuan desert, NM, USA. Results indicate that the horizontal mass flux of wind-borne sediment increased approximately three times following the fire. The REE-tracer analysis of aeolian sediments shows that an average 88% of the horizontal mass flux in the control area was derived from bare microsites, whereas at the burned site it was derived from shrub and bare microsites, 42% and 39% respectively. The vegetated microsites, which were predominantly sinks of aeolian sediments in the unburned areas, became sediment sources following the fire. The burned areas exhibited a spatial homogenization of sediment tracers, highlighting a potential negative feedback on landscape heterogeneity induced by shrub encroachment into grasslands. Though fires are known to increase aeolian sediment transport, accompanying changes in the sources and sinks of wind-borne sediments likely influence biogeochemical cycling and land degradation dynamics. Our experiment demonstrated that REEs can be used as reliable tracers for field-scale aeolian studies.

## ACKNOWLEDGMENTS

I would like to thank Jon Erz, Scott Collins, and Amaris Swann at Sevilleta National Wildlife Refuge. All of your hospitality at the field station was greatly appreciated. You made our stay in NM a comfortable and productive experience. Without the FWS fire crew none of this research could be possible. It is thanks to them that I am able to write my thesis.

Thanks so much to Shelah Cox for being an overall amazing individual and helping me flourish as both an undergraduate and a graduate student. You provide all the guidance, support, candy, and smiles that this department needs.

I learned so much working in the field with Scott Van Pelt, Junran Li, Joel Sankey, Howell Gonzales, and Guan Wang. Thank you all for providing guidance and support throughout my whole research experience. I hope to work with you all again soon.

Thank you to Dr. Sujith Ravi, my advisor, mentor, and overall science hero. Your help throughout my master's program has been invaluable. You've taught me how to be a good scientist and I hope to go on to make you proud.

Thank you to Dr. "G" David Grandstaff and Dr. Ilya Buynevich for all their help throughout my masters and being on my committee. Your support and guidance was vital to my success and I couldn't have done it without you both.

Finally, thank you to Alyssa Finlay, my geo "mom", who brought me into this department and started me on the path to becoming a geologist.

This research was funded by the U.S. National Science Foundation (NSF) Award EAR-1451518 to S. Ravi and the Sevilleta LTER Summer Research Fellowship to D. Dukes.

# TABLE OF CONTENTS

	<b>PAGE</b>
ABSTRACT.....	ii
ACKNOWLEDGEMENTS.....	iii
LIST OF FIGURES.....	vi
LIST OF TABLES.....	x
CHAPTER 1: INTRODUCTION.....	1
CHAPTER 2: BACKGROUND.....	5
2.1 Aeolian Transport.....	5
2.2 Woody Plant Encroachment.....	9
2.3 Fire in Dryland Landscapes.....	12
2.4 Rare Earth Element Tracers.....	14
CHAPTER 3: OBJECTIVES AND HYPOTHOSIS.....	16
3.1 Hypotheses.....	16
3.2 Objectives.....	17
CHAPTER 4: METHODS.....	18
4.1 Study Site.....	18
4.2 Experimental Setup.....	19
4.3 Wind Erosion Monitoring.....	22
4.4 Soil Analysis.....	26
4.5 Rare Earth Element Tracers.....	27
CHAPTER 5: RESULTS.....	30
CHAPTER 6: DISCUSSION.....	52

CHAPTER 7: CONCLUSION.....	57
REFERENCES CITED.....	59
APPENDIX A: DATA.....	68

## LIST OF FIGURES

	PAGE
Figure 1: Aeolian transportation mechanisms due to soil size. ....	6
Figure 2: These are the forces which act on a particle at the threshold shear velocity from <i>Ravi et al.</i> (2011). O is the particle's center of gravity, P is the pivot point of particle entrainment, $F_d$ is aerodynamic drag, $F_l$ is the lift force, $F_g$ is the force due to gravity, and $F_i$ represents interparticle cohesive forces. ....	7
Figure 3. Depiction of the two interparticle forces due to water content ( <i>Ravi et al.</i> , 2011). When the relative humidity is less than 65% (air-dry) the adsorption force dominates. When the relative humidity is greater than 65% the liquid bridge dominates. ....	8
Figure 4. This global map shows the locations of reported woody plant encroachment (blue dots), regions of desert vegetation (yellow), fire affected areas (Red), and the regions in which fire and desert vegetation overlap (orange) ( <i>Ravi et al.</i> , 2009a). ....	11
Figure 5. Sediment is preferentially eroded from bare and grass sites and deposited under shrub sites via canopy trapping ( <i>Ravi et al.</i> , 2007). ....	11
Figure 6. Major biomes of New Mexico. This map was made with data from the New Mexico Resource Geographic Information System. ....	19
Figure 7. (a) The prescribed fire at the shrub-grass transition zone in Sevilleta National Wildlife Refuge, NM. (b) The burned area with one replicate plot showing the experimental set-up and instrumentation in the field. Photo by Sujith Ravi. ....	21
Figure 8. The Modified Wilson and Cooke sediment sampler is used to estimate the horizontal mass flux of aeolian sediment. Samplers are nominally arranged at four different heights, 0.1, 0.25, 0.5, and 1.0 m. ....	23
Figure 9. (a) A 4.5 mm diameter copper sphere is fired at 45° approximately 25 cm from the soil surface. (b) A penetrometer is applied to the soil surface at a 45° angle to gauge the surface resistance to disturbance. (c) This is the typical shape of a disturbance created by the air gun. The long and short diameter are measured and used to calculate the disturbance area. ....	26
Figure 10. The particle size distribution for the three different microsite types. Grasses are denoted by the blue circles, bare sites by the red triangles, and the shrub sites by the green squares. Each cover type displays a bimodal distribution which coarsens from bare sites to grass sites to shrub sites. ....	31

Figure 11. X-ray powder diffractogram of a Sevilletta soil sample made up of quartz, orthoclase, and calcite. ....	32
Figure 12. Notched box plots of VWC from the burned (red) and the control (green). Outliers are represented with red (burned) and blue (control) dots. Significant differences were established thorough the Kruskal-Wallis test with a 95% confidence limit. Significantly different groups are denoted with the alphabetical symbols A, B, C, and D. ....	34
Figure 13. The VWC of the control plot through time (90 day of the windy season). Bare sites are in orange, grass sites in green and shrub sites are in blue. The large increases in VWC are precipitation events. The small oscillations in VWC are diel variations. ....	35
Figure 14. The VWC of the burned area varies with time (90 days of the windy season). The orange line represents the bare site, green is the grass site, and blue is the shrub site. Large increases in VWC are precipitation events. Small oscillations in VWC are diel variations. ....	36
Figure 15. Notched box plots show the daily average wind speed at varying heights in the burned and control areas over a period of 90 days. The burned areas are denoted in red and control are denoted in green. The blue and red points represent outliers and the letters A, B, C, and D show significantly different groups. Burned area wind speeds are consistently greater than control area wind speeds. The difference becomes significant at 0.5 m. ....	37
Figure 16. Notched box plots of the surface wind shear (U) in both the burned and the control plot. Both were found to differ significantly using a T-test with a 95% confidence limit. The red points represent outliers. ....	38
Figure 17. (a) The derived total HMF (Q) from MWAC sediment samplers in the control and burned plots show an average of $27.1 \pm 2.4$ and $75.3 \pm 55.0 \text{ g m}^{-1} \text{ day}^{-1}$ respectively. The control and burned flux are significantly different as shown by the box plots and the Kruskal-Wallis One-Way ANOVA on Ranks statistical test. Significant difference is denoted by the A and B symbols. The red point represents an outlier. (b) The TSV ( $u^*$ ) of bare, grass, and shrub sites was derived using measured surface resistances. Grass and shrub TSVs ( $u^*$ ) decreased significantly following fire and bare sites remained constant as shown by Kruskal-Wallis Multiple Comparison Z-Value test at a 95% confidence limit. Significant differences are indicated by the differing symbols, C, D, and E. Red points are outliers assuming a normal distribution. ....	41

- Figure 18. The mean background concentration of REEs in the soil for each microsite type. The light REEs are much more abundant than the heavier REEs. Eu, Ho, and Yb were chosen as tracers because of this. ....42
- Figure 19. The shale normalized (NASC) spiked REE concentrations as well as the background REE concentrations (*Gromet et al.*,1984). The graph is plotted on a log scale. Each of the spiked REEs is greater than 100 times the background concentration. ....44
- Figure 20. A ternary plot of control area weight percent element composition normalized to the spiked REE concentrations (equation 9) shows mixing between three end members; bare (Yb), grass (Eu), and shrub (Ho). Red dots at or near the vertices indicate that the initial spiked concentrations of these REE are more than 100 times background values at time zero. Orange dots display the composition of bare samples after 90 days, green dots are grass samples (90 days), light blue dots are shrub samples (90 days), and the dark blue triangles show the composition of sediment taken from the MWAC samplers. The data points which plot along or near the bare-shrub and bare-grass axes and the dark blue triangles which plot in the bare corner indicate that the main sediment source is from bare patches and there is limited sediment mixing between the shrub and grass sites.....46
- Figure 21. A ternary plot of burned area weight percent element composition normalized to the spiked REE concentrations (equation 9) shows mixing between three end members; bare (Yb), grass (Eu), and shrub (Ho). Red dots at or near the vertices indicate that the initial spiked concentrations of these REE are more than 100 times background values at time zero. Orange dots display the composition of bare samples after 90 days, green dots are grass samples (90 days), light blue dots are shrub samples (90 days), and the dark blue triangles show the composition of sediment taken from the MWAC samplers. Green and light blue data points plot farther away from the bare-shrub and bare-grass axes and the dark blue triangles plot predominantly along the bare-shrub axis indicating that the main sediment source is from the bare and shrub patches and that there is mixing between all three microsite types. ....47
- Figure 22. Box plots compare tracer REE concentrations in bare microsites between spiked, control and burned plots. Red points are outliers assuming a normal distribution. (a) Bare tracer (Yb) concentrations are not significantly different ( $P > 0.05$ ) in the three sites as indicated by the A symbol. (b) The grass tracer (Eu) concentrations are significantly greater in the burned site than in the control and original spiked plot as indicated by the C symbol. (c) The shrub tracer (Ho) concentration is also significantly greater in the in the burned plot than in the control and original spiked plot as indicated by the E symbol. ....48
- Figure 23. Box plots compare tracer REE concentrations in grass microsites between spiked, control and burned plots. Red points are outliers assuming a normal distribution. (a) Bare tracer (Yb) concentrations in grass sites are significantly

greater in the burned and control plots than the spiked as indicated by the B symbol. (b) The grass tracer (Eu) concentrations are not significantly different ( $P > 0.05$ ) in the three plots as indicated by the C symbol. (c) The shrub tracer (Ho) concentrations are significantly greater in the burned plot than the spiked and the control plots as indicated by the E symbol. ....49

Figure 24. Box plots compare tracer REE concentrations in shrub microsites between spiked, control and burned plots. Red points are outliers assuming a normal distribution. (a) The bare tracer (Yb) concentrations in shrub sites are significantly greater in the burned and control plots than the spiked as indicated by the B symbol (b) The grass tracer (Eu) concentrations in shrub sites are significantly greater in the burned plot than in the spiked and the control plots as indicated by the D symbol. (c) The shrub tracer (Ho) concentration in the shrub sites is not significantly different ( $P > 0.05$ ) between all three plots as indicated by the E symbol. ....50

Figure 25. Box plots comparing vegetative tracer (Ho and Eu) concentrations in all three burned plot microsites. Based on the Kruskal-Wallis test, Ho concentrations in the grass site (A) are significantly greater than in the other sites (B). Red points are outliers assuming a normal distribution. ....51

## LIST OF TABLES

	<b>PAGE</b>
Table 1. Percent distribution of particle sizes in the three different micro sites. ....	30
Table 2. The horizontal mass flux from both the treatment areas (burned and control) as well as the vertical dust flux derived from the percent clay content in the soil. ...	39
Table 3. Calculated TSV of the soil surface under each microsite type obtained using an air rifle method. The values are averaged to show the mean TSV, the standard deviation, and coefficient of variation is also presented. ....	40
Table 4. The average background concentrations of REEs in Sevilleta soil. ....	43

## CHAPTER 1: INTRODUCTION

Population increase, over-exploitation of land and water resources, disturbances such as fire, and climatic changes have rendered drylands worldwide highly susceptible to land degradation, often referred to as “desertification” (*Darkoh, 1998; D’Odorico et al., 2013*). Considering the global significance of drylands on the world’s food security and environmental quality (~40% of the Earth’s terrestrial surface, supporting a population exceeding 2 billion), understanding the biophysical and human dimensions of land degradation is critical (*UNCCD, 1994; Millennium Ecosystem Assessment, 2005*). Accelerated soil erosion by hydrologic and aeolian processes is thought to be responsible for more than 87% of degraded lands, and is often regarded as a cause and effect (positive feedback loop) of desertification (*Middleton and Thomas, 1997; Lal, 2001*). Even though water is by far the dominant soil erosion process globally, in dryland ecosystems soil erosion by wind (aeolian abrasion and deflation) often becomes the dominant erosional process (*Breshears et al., 2003; Ravi et al., 2010b*).

Wind erosion and associated dust emissions play a fundamental role in many ecological processes and provide important biogeochemical connectivity at scales ranging from individual plants to the dynamics of global ecosystems (*Okin and Gillette, 2001; Burkhardt, 2010; Field et al., 2010*). At the local scale, accelerated wind erosion results in loss and redistribution of soil resources and mechanical injury to growing plants (*Retta et al., 2000; Van Pelt and Zobeck, 2007*). The dust emissions have large-scale impacts and affect human health, biogeochemical cycles, precipitation processes and climate (*Field et al., 2010; Ravi et al., 2011*). Furthermore, increases in rates of wind erosion and dust emissions resulting from increased aridity (climatic changes) may result in enhanced loss

of soil resources and a decline in vegetation cover (*Munson et al.*, 2011; *Ravi et al.*, 2011). As vegetation exerts a dominant control on wind erosion, vegetation shifts (grass-shrub transitions, exotic grass invasions) and disturbances to vegetation, such as wildfires, can greatly enhance the transport and redistribution of soil resources by wind (*Whicker et al.*, 2002; *Sankey et al.*, 2009,2013; *Miller et al.*, 2012).

Grasslands and rangelands in arid and semi-arid regions of the world, which provide fundamental ecosystem services, are undergoing rapid increases in fire activity and are highly susceptible to post-fire accelerated soil erosion by wind (*Bowman et al.*, 2009; *Sankey et al.*, 2009; *Ravi et al.*, 2010a; *Miller et al.*, 2012). A common form of land degradation in drylands is the encroachment of woody plants into areas historically dominated by grasses. This phenomenon is observed worldwide (North America, South America, Africa, Asia, and Australia) and is often referred to as “shrub encroachment” (*Schlesinger et al.*, 1990; *Ravi et al.*, 2009a, b). Several studies have investigated the ecohydrological and biogeochemical implications of this transformative ecosystem change (*Huxman et al.*, 2005; *Li et al.*, 2007, 2008; *Turnbull et al.*, 2012). Shrub encroachment is thought to contribute to land degradation by increasing the amount of bare soil, which can be eroded by wind (*Okin and Gillette*, 2001; *Gillette and Pitchford*, 2004) and allows for soil nutrients to be stripped from unvegetated areas and partially redistributed via canopy trapping onto shrub patches (*Schlesinger et al.*, 1990; *Li et al.*, 2008). This creates a self-sustaining cycle of erosion, depletion of soil nutrients, and loss of grass cover (*Archer et al.*, 1995). The loss of grasses decreases the pressure of fires on shrub vegetation thereby further enhancing woody plant encroachment. The resulting landscape is characterized by hydrologically and nutritionally enhanced shrub islands (or “islands of fertility”), which

are sediment sinks, and nutrient depleted bare interspaces that act as sediment sources (*Schlesinger et al.*, 1990).

Fires are common in many shrub-grass transition systems, and important feedbacks are known to exist among wind erosion, vegetation change, and fires, in the context of land degradation (*Li et al.*, 2007, 2008; *Sankey et al.*, 2009, 2012b; *Ravi et al.*, 2010a). In the grass-shrub ecotones of the Chihuahuan desert in the Southwestern US recent studies have demonstrated that by altering soil erosion processes at the early stages of shrub encroachment, fires can play an important role in the local-scale redistribution of soil resources within the landscape (*Ravi et al.*, 2010a; *Sankey et al.*, 2012a; *Van Pelt et al.*, 2017b). On low-relief surfaces, fires can induce rapid changes in soil surface characteristics, remove vegetation cover, and increase erosion and nutrient redistribution (*Paysen et al.*, 2000; *Whicker et al.*, 2002; *Ravi et al.*, 2009a, 2010a). Furthermore, burning of vegetative biomass at the surface can induce soil hydrophobicity, which has been shown to enhance post-fire soil erosion by decreasing the interparticle forces due to moisture in soils (*DeBano*, 1966; *Ravi et al.*, 2006, 2007). Recent studies using wind tunnels and small-scale field experiments have qualitatively demonstrated that in shrublands and shrub-grass transition zones fires can enhance soil erosion under shrub vegetated microsites and result in some level of resource redistribution to the interspaces (*White et al.*, 2006; *Ravi et al.*, 2009a; *Sankey et al.*, 2012a,b,c). Even though this fire-erosion feedback has the potential to homogenize the landscape (*Sankey et al.*, 2010, 2012a, b), the actual extent of post-fire soil redistribution and homogenization is poorly understood. This is a critical research gap, as quantifying the post-fire redistribution and loss of soil resources is important in evaluating the benefits of using prescribed fires as a tool for grassland habitat management.

A quantitative assessment that integrates fire-wind erosion feedbacks is therefore urgently needed for understanding land degradation dynamics, vegetation change, soil biogeochemical cycling, air quality, and landscape evolution. However, this quantification is challenging, partly due to the lack of reliable tracer-based techniques to precisely determine the rate of soil erosion and redistribution or to reconstruct the aeolian source-to-sink routes. Several studies have used tracers, such as oxides of rare earth elements (REEs), to quantify water erosion rates (*Zhang et al.*, 2001; *Polyakov et al.*, 2004; *Zhu et al.*, 2011; *Guzmán et al.*, 2013). These studies showed that soil redistribution patterns, erosion and aggregation, can be tracked with REE tracers (*Zhang et al.*, 2001). However, studies on quantifying wind erosion using REE traces are limited (e.g. *Van Pelt et al.*, 2012, 2014, 2017b).

Preliminary studies on tracer applications for wind erosion have led to the development of REE application protocols for tracking aeolian redistribution of surface sediments at the plot scale using field wind tunnel studies (*Van Pelt et al.*, 2012, 2014, 2017b). Here, we add to the existing studies by investigating the applicability of this tracer technique – the novel use of multiple REE tracers to quantify field-scale soil erosion by wind and to identify sources and sinks of wind-blown sediments in a fire affected, desert shrub-grass ecotone. We hypothesize that vegetation microsites (shrub or grass patches), which are sinks of aeolian sediments in arid landscapes, may act as enhanced sediment sources following fires. This post-fire modification of sediment sources and sinks in the landscape might impact rates of resource redistribution and soil patterning, therefore leading to a more homogeneous landscape.

## CHAPTER 2: BACKGROUND

### 2.1 Aeolian Transport

Aeolian processes, which include the erosion, transport and deposition of sediments by wind, involve natural geomorphic and sedimentological mechanisms. However, rapid and persistent shifts in climate, disturbances to vegetation cover, and anthropogenic activities can greatly accelerate wind-borne sediment transport. The physical mechanisms underlying wind erosion are well understood (*Okin et al.*, 2006; *Ravi et al.*, 2011; *Kok et al.*, 2012).

Bagnold (1941) defined the three distinct mechanisms of transport by wind as soil creep (or occasional reptation), saltation, and suspension (Figure 1). These mechanisms are largely controlled by grain size with large sand sized particles ( $>500 \mu\text{m}$ ) transported by creep, smaller particles ( $20\text{-}500 \mu\text{m}$ ) by saltation, and silt and clay sized particles ( $<20 \mu\text{m}$ ) transported by suspension and typically standardized for threshold near-surface wind velocities of  $5 \text{ m/s}$  (*Bagnold*, 1941). These different mechanisms of sediment transport are responsible for the redistribution of soil resources at different scales. For example, saltation is the primary process that moves materials at the plant-interspace to field scales, whereas suspension is responsible for the movement of fine material (dust) at regional to global scales via the process of long-range transport (*Okin et al.*, 2006). The two dimensions of aeolian transport are the horizontal mass flux (HMF) ( $Q$ ), the primary, local redistributor of sediment mostly consisting of saltating and creeping particles (*Larney et al.*, 1998), and the vertical dust flux ( $F_e$ ), which consists of small particles that have been suspended in air currents. Suspended dust particles can be transported and deposited over large areas (*Shao et al.*, 1993; *Swap et al.*, 1996).

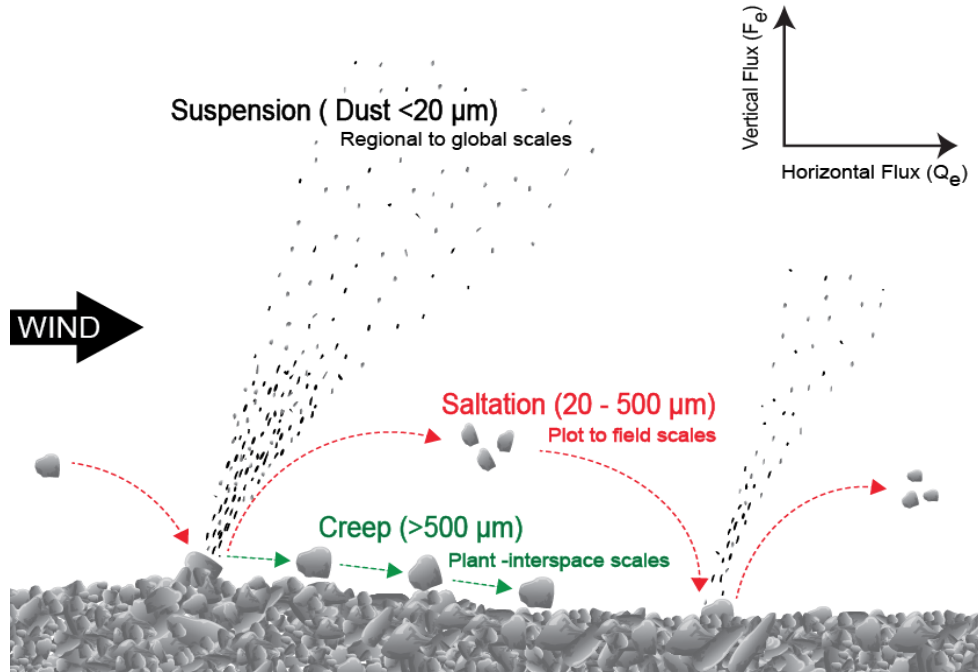


Figure 1. Aeolian transportation mechanisms due to soil size.

Wind erosion is initiated when the force of the wind exceeds the threshold shear velocity (TSV) of the soil, the minimum velocity needed for erosion to occur. TSV is affected by several factors including soil texture and moisture content, as well as sheltering effects of vegetation. The TSV of soil is determined by a balance of forces - aerodynamic and stabilizing forces - at the threshold point of entrainment (Figure 2). Aerodynamic forces are made up of the drag force ( $F_d$ ) and the lift force ( $F_l$ ) (Shao, 2008). The stabilizing forces are composed of the normal force due to gravity ( $F_g$ ) and interparticle cohesive forces ( $F_i$ ). Sediment particles are entrained and transported by wind at a critical TSV where the aerodynamic forces exceed stabilizing forces.

Bagnold's (1941) theoretical model predicts the TSV ( $u_t$ ) of dry, spherical particles that are only affected by gravitational forces and aerodynamic drag:

$$u_t^* = A \sqrt{\frac{(\rho_s - \rho_a)}{\rho_a} g d} \quad (1)$$

where  $A$  is a dimensionless threshold parameter,  $\rho_s$  is the particle density,  $\rho_a$  is the air density,  $g$  is gravitational acceleration, and  $d$  is the mean diameter of the particle (Bagnold, 1941). However, Bagnold's (1941) model breaks down for particles underneath the critical grain size of  $60 \mu\text{m}$  where interparticle cohesive forces cause the soil TSV to increase (Iversen and White, 1982; Marticorena and Bergametti, 1995). Over the years Bagnold's (1941) model has been modified to accommodate the effect of interparticle cohesive forces, soil moisture, and the sheltering effect of vegetation (Cornelis et al., 2004; Ravi et al., 2006; Okin, 2008).

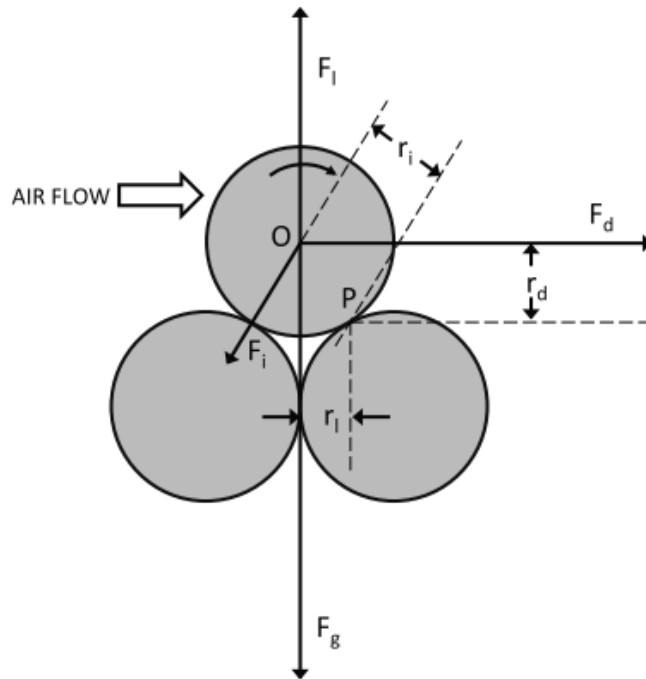


Figure 2. These are the forces which act on a particle at the threshold shear velocity from Ravi et al. (2011). O is the particle's center of gravity, P is the pivot point of particle entrainment,  $F_d$  is aerodynamic drag,  $F_l$  is the lift force,  $F_g$  is the force due to gravity, and  $F_i$  represents interparticle cohesive forces.

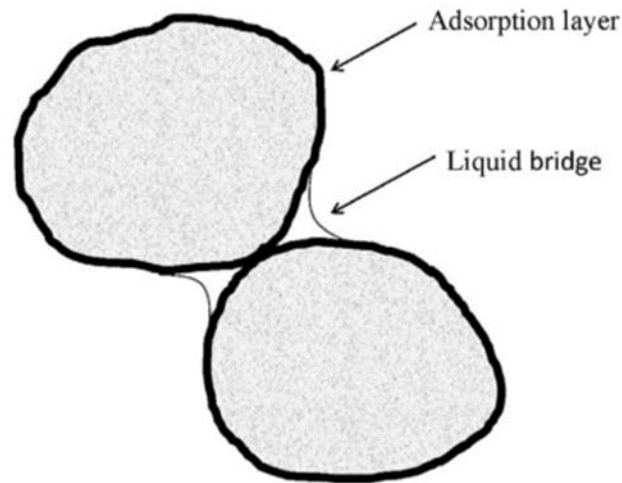


Figure 3. Depiction of the two interparticle forces due to water content (*Ravi et al.*, 2011). When the relative humidity is less than 65% (air-dry) the adsorption force dominates. When the relative humidity is greater than 65% the liquid bridge dominates.

Soil moisture, through the interparticle cohesion forces created by soil water retention, can add to stabilizing forces and change the TSV on short time scales (e.g. diurnal) (*Chepil*, 1956; *Shao*, 2008; *Ravi et al.*, 2011). Soil moisture can either form a “liquid bridge” in soil particle interspaces or it can be adsorbed to the particle surfaces (Figure 3) (*Ravi et al.*, 2006). Soil texture and saturation govern which type of interparticle cohesive force, a liquid bridge or an adsorbed layer, is dominant (*Haines*, 1925; *Ravi et al.*, 2011). In wet sandy soils the liquid bridge is the principle cohesive force, whereas wet clayey soils tend to experience a greater cohesive force from an adsorbed layer (*Haines*, 1925). In air-dry soils the effect of texture is negligible and the adsorption force always dominates (*Haines*, 1925).

Vegetation can act as a nonerodable roughness element which shelters soil by lowering surface wind velocity (*Stockton and Gillette*, 1990; *Ravi et al.*, 2011). Surfaces

with greater roughness tend to have significantly higher TSVs than that of smooth surfaces (Gillette and Stockton, 1989). Thus, as the surface roughness provided by vegetation increases so too does the sheltering effect it provides (Stockton and Gillette, 1990). If vegetation were to be removed by disturbance mechanisms such as fire or grazing the TSV would then decrease allowing for the entrainment and transport of soil particles (Stockton and Gillette, 1990; Ravi et al., 2009a; Van Pelt et al., 2017a).

In dryland systems, the dominant controls over wind erosion are vegetation and soil moisture. Vegetation cover lowers the momentum of wind at the soil surface sheltering it from erosion (Stockton and Gillette, 1990), whereas soil moisture contributes to inter-particle forces that increase the threshold velocity needed for entrainment and transport (Chepil, 1956; Ravi et al., 2006). Thus vegetation shifts (grass-shrub transitions) and disturbances (wildfires) can greatly accelerate the transport and redistribution of soil resources by wind. A case in point is the grass-shrub ecotones in the Chihuahuan desert, where interactions among aeolian processes, vegetation, and fires are thought to play a major role in the rapid encroachment of shrubs and associated land degradation (D'Odorico et al., 2012).

## **2.2 Woody Plant Encroachment**

The encroachment of woody plants into areas historically dominated by grasses, which often coincides with land degradation processes, is observed in many dryland systems worldwide (often referred to as “shrub encroachment”) and has ecological, hydrologic, and biogeochemical consequences (Schlesinger et al., 1990; Huxman et al., 2005; Ravi et al., 2009a) (Figure 4). Shrub encroachment has been observed in the desert

margins of North America, South America, Africa, Asia, and Australia (*Ravi et al.*, 2009a) (Figure 4). The encroachment process is attributed to a complex interaction among several factors including warming, fire suppression, overgrazing, and increased atmospheric CO<sub>2</sub> (*Buffington and Herbel*, 1965; *Schlesinger et al.*, 1990; *Gibbens et al.*, 2005). Shrub encroachment is thought to contribute to land degradation by increasing the amount of bare soil which can be eroded by wind (*Gillette and Pitchford*, 2004) and allows for soil nutrients to be stripped from unvegetated areas and partially redeposited via canopy trapping onto shrub patches (*Schlesinger et al.*, 1990) (Figure 5). This creates a positive feedback cycle of erosion, depletion of soil nutrients, and loss of grass cover (*Archer et al.*, 1995). The loss in grass fuel decreases the pressure of fires on shrub vegetation thereby further enhancing woody plant encroachment. The resulting landscape is characterized by nutrient-rich shrub “islands of fertility”, which are sediment sinks and nutrient-poor bare interspaces that act as sediment sources (*Schlesinger et al.*, 1990). Aeolian processes are largely responsible for enhancing and maintaining shrub “islands of fertility” and associated accelerated soil erosion is thought to be both a cause and effect of land degradation (*Ravi et al.*, 2009b). A majority of woody plant encroachment occurs in desert margins which are highly susceptible to disturbances such as fires (*Ravi et al.*, 2009a). *Ravi et al.* (2009a) proposed that interactions between wind and fire, which removes shrubs, may provide a feedback mechanism to woody plant encroachment by disrupting and reversing the formation of the shrub “islands of fertility”.

A patchy mixture of bare soil microsites and vegetated microsites is common in dryland ecosystems consisting of either shrubland or grassland (*Ravi et al.*, 2011). Grassland bare patches are mostly on the decimeter scale, whereas shrubland bare patches

can range up to a few meters (*Nash et al.*, 2004). This patchiness is thought to be attributed to competition for and the limitation of resources, specifically water (*D'Odorico et al.*, 2006). A shift from grassland to shrubland, which is characterized by an increase in bare patches, can be abrupt and irreversible as both ecosystems are the alternative attractors of a bistable system (*Westoby et al.*, 1989; *Anderies et al.*, 2002; *D'odorico et al.*, 2012, 2013). Overall, this transition from a grassland to a shrubland produces an increase in bare soil surface which can then be eroded, accelerating the land cover change (*Schlesinger et al.*, 1990; *Huenneke et al.*, 2002).

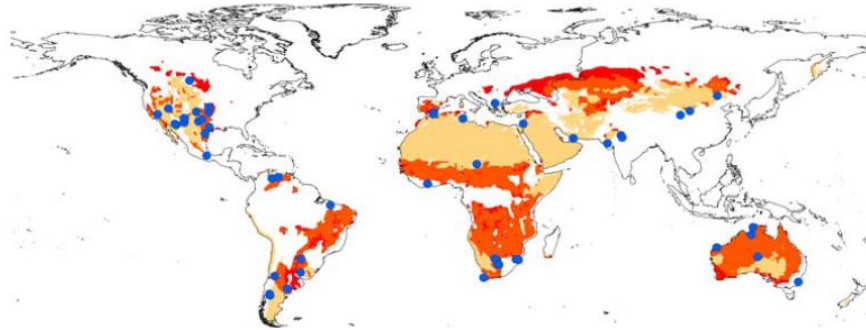


Figure 4. This global map shows the locations of reported woody plant encroachment (blue dots), regions of desert vegetation (yellow), fire affected areas (Red), and the regions in which fire and desert vegetation overlap (orange) (*Ravi et al.*, 2009a).



Figure 5. Sediment is preferentially eroded from bare and grass sites and deposited under shrub sites via canopy trapping (*Ravi et al.*, 2007).

Infiltration, runoff, and evapotranspiration are three hydrologic processes influenced by vegetation type and density (*Dunne, 1978; Casenave and Valentin, 1992; Huxman et al., 2005*). Hortonian runoff, which occurs when the precipitation rate exceeds the capacity for infiltration, is more common in semiarid regions with thin vegetation often influenced by overgrazing, whereas saturation excess, which results from an excess of water greater than that which can be stored in the soil, is dominant in regions with denser vegetation and limited soil storage capacity (*Horton, 1933; Dunne, 1978; Casenave and Valentin, 1992*). With the development of soil crusts and an increase in vegetation density the runoff of a region also increases (*Casenave and Valentin, 1992*). Invasive woody plants tend to have deeper roots which, depending on the location (riparian zone) and seasonality, can lower the water table adjacent to streams and rivers thus reducing both baseflow and discharge (*Huxman et al., 2005*). Woody plant encroachment, through an increase in bare surface cover, may also increase the evaporation component of evapotranspiration (*Huxman et al., 2005*). The impact of woody plant encroachment on the hydrologic cycle is extensive and can influence processes of sediment transport. Feedback mechanisms for woody plant encroachment need to be identified to develop best management practices for impacted regions.

### **2.3 Fire in Dryland Landscapes**

Many drylands are undergoing changes in fire regimes and increased fire frequency as a result of climate change and human activities (*Bowman et al., 2009*). Grass-shrub transition regions are affected by fire occurrences, as a sufficient amount of grass biomass exists to carry the fires from the points of ignition to the surrounding vegetation. Under

these conditions fires can alter the source-sink sediment dynamics in a grass-shrub system. Recent studies have demonstrated that by altering soil erosion processes at the early stages of shrub encroachment fire can play an important role in the local-scale redistribution of soil resources within the landscape. On low-relief surfaces, fires can induce rapid changes in soil surface characteristics (*Paysen et al.*, 2000; *Ravi et al.*, 2009a), remove vegetation cover, and produce an increase in erosion and nutrient redistribution (*Whicker et al.*, 2002; *Ravi et al.*, 2009a). Further, burning of vegetative biomass at the surface can induce soil water-repellency (or soil hydrophobicity) which has been shown to enhance post-fire soil erosion by decreasing the interparticle forces due to moisture in soils (*Ravi et al.*, 2006, 2007).

Fire volatilizes organic compounds in vegetation causing, through a strong temperature gradient, the volatilized gasses to be pulled down into the soil column where they condense on the surface of soil particles making them hydrophobic (*DeBano*, 2000). Fire related hydrophobicity, by increasing the contact angle of the air/water interface above 90°, causes a positive capillary pressure allowing water to rest at the soil surface rather than be drawn down (*Letey*, 2001). These mechanisms have been linked to decreases in infiltration and increases in runoff which can in turn impact erosion and the redistribution of water and nutrients (*Krammes and DeBano*, 1965; *Schlesinger et al.*, 1990; *Ravi et al.*, 2007).

Overall, disturbances, such as natural and anthropogenic fires, can greatly accelerate the rate of soil erosion in drylands by altering vegetation cover and soil hydrologic properties. The post-fire aeolian transport of sediments is thought to be a significant driver of nutrient and contaminant export from these systems. In landscapes

undergoing rapid vegetation shifts, as in the grasslands of Chihuahuan desert, the fire-erosion feedback can alter the source-sink dynamics and sediment fluxes from these systems. Recent studies using wind tunnels and small-scale field experiments have qualitatively demonstrated that in shrub-grass transition zones fires can enhance soil erosion under shrub vegetated microsites and result in some level of resource redistribution to the interspaces (*Ravi et al.*, 2009a). Even though this fire-erosion feedback has the potential to homogenize the landscape, the actual extent of post-fire soil redistribution and homogenization is poorly understood and a quantitative understanding of rates of post-fire aeolian sediment transport is still missing due to the lack of reliable field techniques.

#### **2.4 Rare Earth Element Tracers**

The REE group or lanthanides is made up of 15 elements with the atomic numbers 57 to 71. REEs can be further broken into two separate groups based on atomic weight: the light REEs (atomic number 57 – 64) and the heavy REEs (64 – 71) (*Van Gosen et al.*, 2014). REEs do not tend to concentrate in ore bodies except in uncommon rock types, but they can be regularly found in soils at concentrations in the tens of parts per million with the even periodic numbered REEs being more abundant than the odd (*Markert*, 1987). REEs have a low environmental toxicity, low mobility in alkaline soils, and bind strongly to soil particles (*Wytenbach et al.*, 1998; *Land et al.*, 1999; *Zhang et al.*, 2001). These properties make REEs ideal as tracers for sediment transport studies.

REEs (added to the soil) have been extensively tested for their tracing abilities for hydraulically transported sediment in both the lab and in the field (*Zhang et al.*, 2001, 2003; *Polyakov and Nearing*, 2004; *Polyakov et al.*, 2004; *Kimoto et al.*, 2006; *Deasy and*

Quinton, 2010). Zhang *et al.* (2001) developed a quick acid-leaching method to quantify REE concentration in soil and, through a series of lab experiments in which REE treated silt loam was leached with deionized water, demonstrated that REEs bind strongly to the soil surface and their use as tracers in the field is feasible. Polyakov and Nearing (2004) showed, through a combination of laser based digital elevation models (DEMs) and multiple REE tracers, that differential erosion and deposition of sediment on hillslopes can be quantified. Deasy and Quinton (2010) successfully used multiple REE tracers in a field setting where they identified sources and sinks of sediment on an agricultural hillslope following rain events. Deasy and Quinton (2010) also developed a non-intrusive spray-application method for REEs (REEs suspended in water) which is in contrast with other methods which physically mixed REEs with the soil particles disturbing the soil surface.

Recent studies have begun to assess REEs as tracers for aeolian transport (Van Pelt *et al.*, 2012, 2014, 2017b). Van Pelt *et al.* (2014) developed protocols to apply REE tracers to the top 2 cm of the soil without disturbing the soil surface or vegetation. Van Pelt *et al.*'s (2014) method is similar to that of Deasy and Quinton (2010), however, it involves the use of nitric acid to dissolve the REEs rather than suspend the REE oxide particles in water. The multi-REE application and tracer method was shown to be successful in wind tunnel experiments (Van Pelt *et al.*, 2014). A single REE tracer field experiment (under stable conditions) was later shown to be a reliable method for tracking aeolian transport. However, field applications of multi-REE tracer techniques under disturbance conditions such as fire have never been assessed before.

## CHAPTER 3: OBJECTIVES AND HYPOTHESIS

The encroachment of woody vegetation into historically grass dominated areas, through increases in aeolian sediment fluxes and landscape heterogeneity, is thought to be a positive feedback loop in a bistable system (*Schlesinger et al.*, 1990; *Ravi et al.*, 2009b; *D'Odorico et al.*, 2013). Accelerated soil erosion, which can be caused by woody plant encroachment, is considered a cause and an effect of desertification (*Schlesinger et al.*, 1990; *Darkoh*, 1998). Changes in land cover, specifically an increase in bare area associated with the grass-shrub transition, reduce aerodynamic roughness at the soil surface and thus decrease the TSV and increase aeolian transport (*Stockton and Gillette*, 1990; *Ravi et al.*, 2009a; *Van Pelt et al.*, 2017a). The transition between a grassland and a shrubland is assisted by anthropogenic influences such as overgrazing and fire suppression (*Schlesinger et al.*, 1990; *Darkoh*, 1998). Whereas wildfires are known to greatly increase aeolian sediment fluxes through removal of vegetation and reduction of moisture-bonding forces in soil, they may provide an important feedback mechanism to woody plant encroachment by inducing sediment redistribution and landscape homogeneity (*Whicker et al.*, 2002; *Ravi et al.*, 2009a; *Sankey et al.*, 2009). However, post-fire sediment redistribution by aeolian transport is poorly quantified. REEs could act as a useful tracing tool to quantify sediment transport and redistribution from multiple land cover types in a shrub grass transition zone.

### 3.1 Hypotheses

- 1) Rare earth elements can be used as reliable tracers to track and quantify sediment transport and redistribution by wind.

- 2) Vegetated microsites, which are generally aeolian sediment sinks within a shrub-grass transition zone, will become active sediment sources post-fire.

### 3.2 Objectives

1. **To quantify the post-fire erosion and dust emissions in a shrub-grass transition zone in the southwestern United States.**

Replicated field experiments will be conducted in burned and unburned areas to quantify the aeolian transport and redistribution of sediments.

2. **To test the applicability of REE oxides as tracers to quantify wind erosion and redistribution.**

REE tracers will be applied in replicate to vegetated and unvegetated microsites in burned and unburned areas. To quantify the loss and redistribution of sediments as well as to identify sediment sources and sinks, extensive soil sampling will be conducted annually and soil REE concentrations will be analyzed in the laboratory.

3. **To observe the effects of fire on wind shear and soil moisture properties.**

Meteorological towers within the burned and control plots measure soil moisture underneath different land cover types and the wind speed from four different heights.

To address these objectives and hypotheses, I investigated the applicability of REE tracer technique to quantify field-scale soil erosion by wind and to identify sources and sinks of wind-blown sediments in a fire affected, desert grassland ecosystem in the Chihuahuan desert of New Mexico. The overall goal is to quantify a field-scale eco-geomorphic (vegetation – fire – erosion) feedback in this shrub-grass ecotone to better understand the complexity of land degradation dynamics.

## CHAPTER 4: METHODS

### 4.1 Study Site

Field experiments were conducted at the Sevilleta National Wildlife Refuge (SNWR) in the northern Chihuahuan Desert approximately 80 km south of Albuquerque, NM (Figure 6). The shrub-grass transition zone is a heterogeneous landscape with a mosaic of mostly black grama grass (*Bouteloua eriopoda* Torr.) and creosote shrub (*Larrea tridentata* (DC.) Cov.) with bare soil interspaces. The land cover in the study area (lat/long: 34.33061916071648, -106.7207788921361) is typical of desert grassland, with ~70–75% grass cover, 20–30% bare interspaces, and a very low density (5–10%) of shrubs (*Báez and Collins, 2008*). In the field site, grasses provide enough connectivity among shrub patches to allow the spread of fire in the presence of strong winds (*Ravi et al., 2009a*). The windy season in this area is from February to May and the prevailing wind is from the southwest (*Ravi et al., 2009a*). Most summer precipitation occurs between June – October, during the North American monsoon (*Higgins et al., 1997*). The soil in the study area is primarily sandy loam (*Johnson, 1988*).

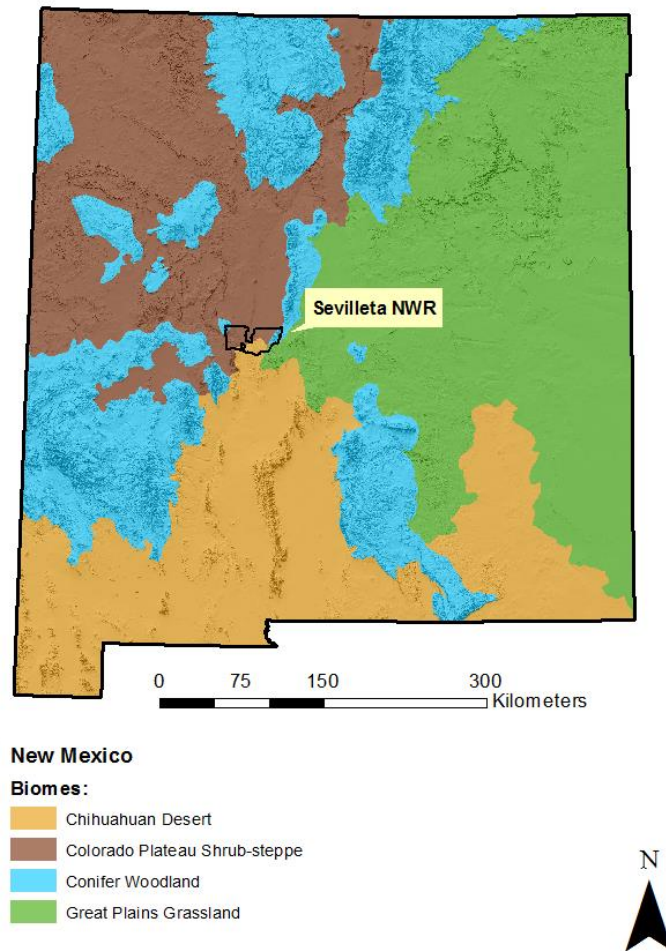


Figure 6. Major biomes of New Mexico. This map was made with data from the New Mexico Resource Geographic Information System.

#### 4.2 Experimental Setup

The experimental site consisted of two 100 x 100 m monitoring areas, one control (unburned) and one burned, which are 250 m apart (Figure 7a). The areas were established at the beginning of the windy season in March 2016 and are characterized by similar soil texture, vegetation and topography. In each monitoring area we established three 30 x 10 m replicate plots (50 m apart) oriented perpendicular to the predominant wind direction

(240°). Line transects were performed to ensure that each plot encompassed the heterogeneity of the landscape (shrub, grass, and bare microsites). In the middle of each of the replicated plots, a 5 x 5 m sampling area was established to conduct the REE-tracer application study. A prescribed fire was conducted in one of the monitoring areas, and was confined inside the area (Figure 7b).

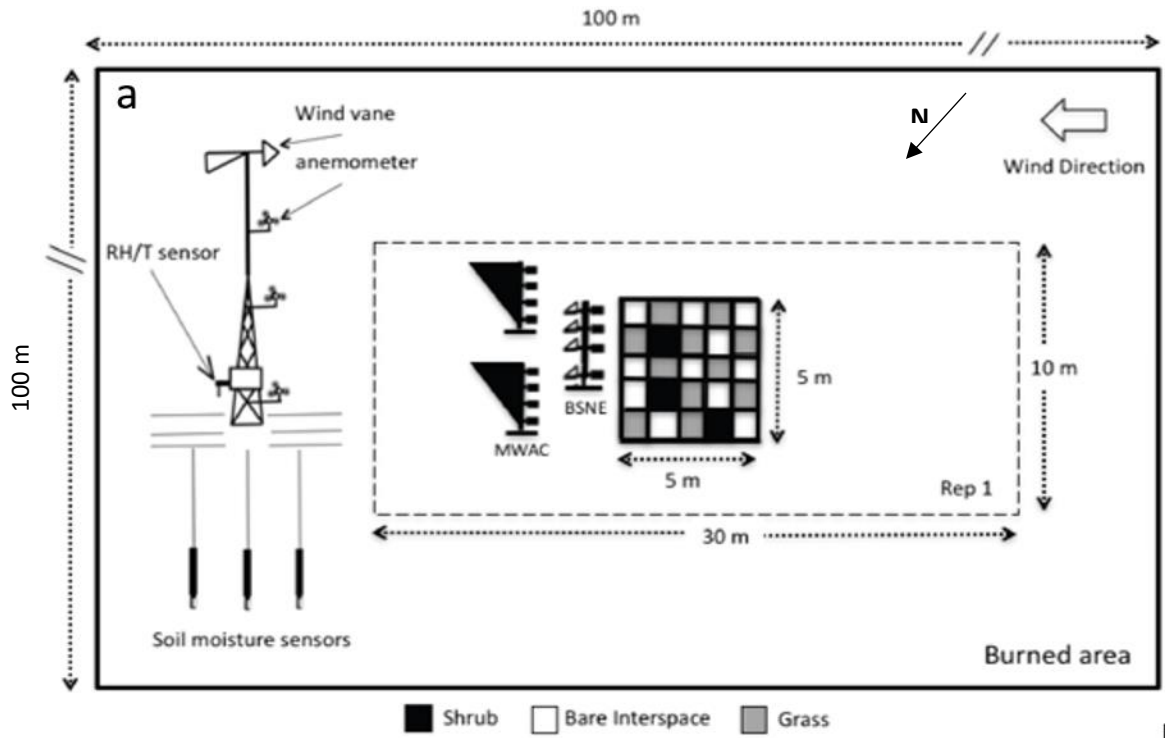


Figure 7. (a) The prescribed fire at the shrub-grass transition zone in Sevilleta National Wildlife Refuge, NM. (b) The burned area with one replicate plot showing the experimental set-up and instrumentation in the field. Photo by Sujith Ravi.

Two identical meteorological towers (Campbell Scientific Instrumentation Tripod CM106) were installed in the burned and control area (Figure 7a). Each solar powered (Campbell Scientific 50 W Solar Panel SP50-L) tower was equipped with a data logger (Campbell Scientific Measurement and Control Datalogger CR1000), and sensors to measure wind speed (Campbell Scientific Wind Sentry Anemometer 03101-L), direction (Campbell Scientific Wind Sentry Set 03002-L), relative humidity, and air temperature (Campbell Scientific Temperature/RH Probe CS215-L). A wireless data acquisition system allowed data to be downloaded remotely. The wind speeds were measured at 4 different heights (arranged exponentially; 0.5, 1.0, 2.0, and 4.0 m). Meteorological variables were sampled every second and averaged over 5 minute intervals. Soil moisture sensors (Campbell Scientific, 12 cm Soil Water Content Reflectometer, CS655) were installed 5 cm below the soil surface in each site – one in each of the shrub, grass, and bare soil microsites in both the burned and control treatments for a total of six sensors.

### 4.3 Wind Erosion Monitoring

The shear velocity ( $u^*$ ) of the wind at the soil surface is determined using the log wind law:

$$u(z) = \frac{u^*}{0.4} \ln \frac{z-d}{z_m} \quad (2)$$

where  $u(z)$  is the wind velocity at various heights,  $z$ ,  $d$  is the zero plane displacement determined by multiplying 0.7 times the height of the larger roughness elements (shrubs),  $z_m$  is the momentum roughness parameter, and 0.4 is the von Karman constant (Campbell and Norman, 1998; Cornelis, 2006). The wind velocities from four

different heights (0.5, 1, 2, and 4 m) in control and burned areas are plotted as a function of the natural log of those height,  $\ln(z-d)$ . A zero plane displacement value of 0.43 is used for the control plots representing the 0.7 times the height of the shrubs (0.62 m). A displacement of 0.0 was used for the burned calculations. A line is fit to the data and the slope of this line,  $m = (u^*/0.4)$ , is then multiplied by the von Karman constant (0.4) to yield the shear velocity (*Campbell and Norman, 1998*).  $Z_m$  is determined by taking the exponent of the negative intercept divided by the slope.

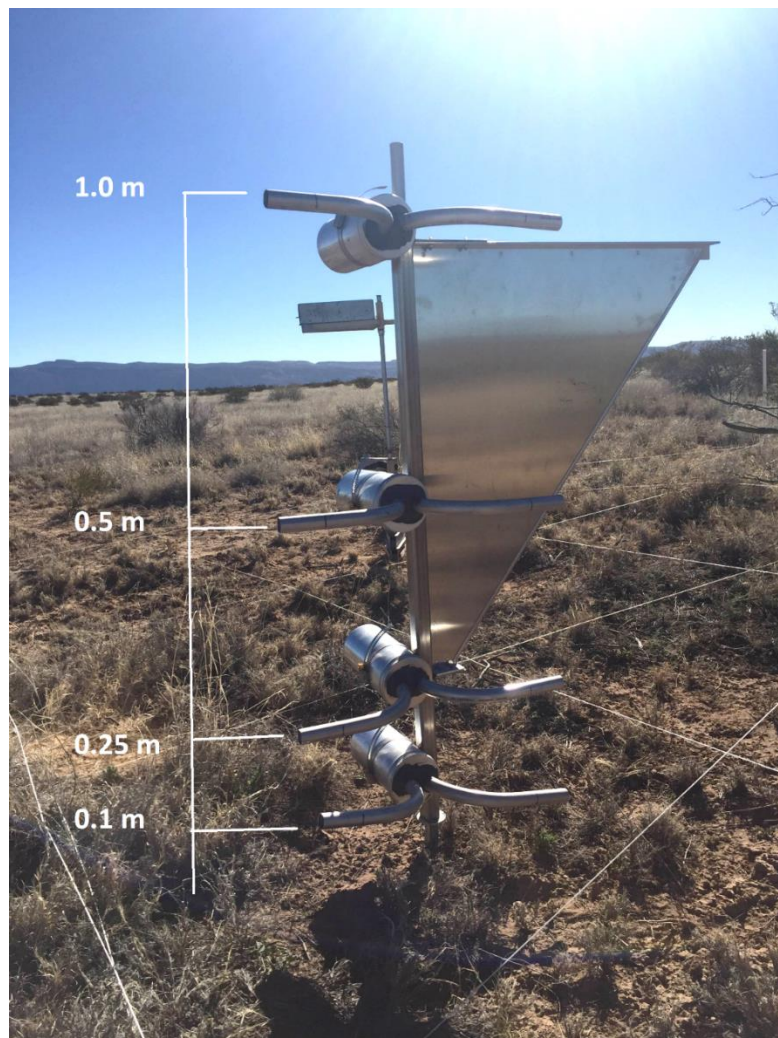


Figure 8. The Modified Wilson and Cooke sediment sampler is used to estimate the horizontal mass flux of aeolian sediment. Samplers are nominally arranged at four different heights, 0.1, 0.25, 0.5, and 1.0 m.

The horizontal mass flux, the major process responsible for soil redistribution by wind, of each monitoring area was quantified using two MWAC (Modified Wilson and Cooke) sediment samplers (isokinetic sediment collectors) per replicate, which were placed at the downwind side of each of the 5 m x 5 m sampling area. The custom-made MWAC sampling systems consist of an array of samplers mounted at four different heights (nominally 0.1, 0.25, 0.5, 1.0 m) attached to pivoting wind vane (Figure 8).

The time-averaged horizontal mass movement,  $q(z)$ , was calculated by dividing the mass of sediment collected in the samplers by the collection interval and the area of the MWAC sampler inlet ( $2.34 \times 10^{-4} \text{ m}^2$ ). The  $q(z)$  results were fit to the widely used empirical formula developed by *Shao et al.* (1993).

$$q(z) = ce^{(az^2+bz)} \quad (3)$$

where  $z$  is the height from the ground to the center of the dust sampler inlet and  $a$ ,  $b$ , and  $c$  are fitting constants. The total horizontal mass flux (HMF),  $Q$ , was calculated by integrating  $q(z)$  from the ground surface to a height of 1 m.

$$Q = \int_0^1 q(z) dz \quad (4)$$

The Vertical dust flux (VDF),  $F_e$ , is linearly related to the total HMF by a soil specific constant,  $k$  ( $\text{m}^{-1}$ ) (*Shao et al.*, 1993; *Gillette et al.*, 1997):

$$F_e = kQ \quad (5)$$

where  $k$ , which typically ranges between  $10^{-3} \text{ m}^{-1}$  to  $10^{-5} \text{ m}^{-1}$ , is determined empirically through an equation developed by *Marticorena and Bergametti* (1995) (where  $k$  is in  $\text{cm}^{-1}$ ):

$$\log(k) = 0.134(\%clay) - 6 \quad (6)$$

The percent clay was determined for each cover type using a laser diffraction particle size analyzer (Beckman Coulter LS 13 320). Because the clay fraction varied between microsite types, the total percent clay for the land surface was derived using the relative area of each microsite type (shrub, grass, and bare), determined by the line transect method.

We estimated the changes in threshold shear velocity (TSV) following fire to examine similarities and differences in sediment supply and erodibility amongst treatment areas (burned and control), and microsites using a recent empirical method developed by *Li et al.* (2010). In this method, to create an empirical equation, the log transformed TSV was related to the resistance of the soil surface to disturbances created by a penetrometer and the disturbance area of a projectile shot by an air gun into the soil surface (Figure 9a, b) (*Li et al.*, 2010). A spherical copper projectile (4.5 mm diameter) was fired from a Crosman Pumpmaster 760 air gun (3 pumps) at the soil surface from an angle of 45° and a height of 25 cm (Figure 9a). This was repeated 10 times in each microsite type of each treatment area, burned and control. The dimensions (maximum diameter and the perpendicular line distance) of the impact disturbance were measured along the long and short axes (Figure 9c). A pocket penetrometer was used to measure the resistance of the soil to compressional force at 45° (Figure 9b). The resulting empirical TSV equation is:

$$u_t^* = \frac{e^{[(1.90654 * P) + (\frac{-0.0781 * A}{100}) + (4.0954)]} + 10}{100} \quad (7)$$

where  $u_t^*$  is the TSV, P is the resistance given by the penetrometer, and A is the area of the surface disturbance caused by the projectile (*Li et al.*, 2010). This method is

easy to apply, allows repeated measurements of TSVs, and therefore captures the spatial and temporal patterns of wind erosion potential on the soil surface post-fire. This method has been successfully applied in many locations around the U.S., including the desert grassland of southern New Mexico (*Li et al.*, 2010).

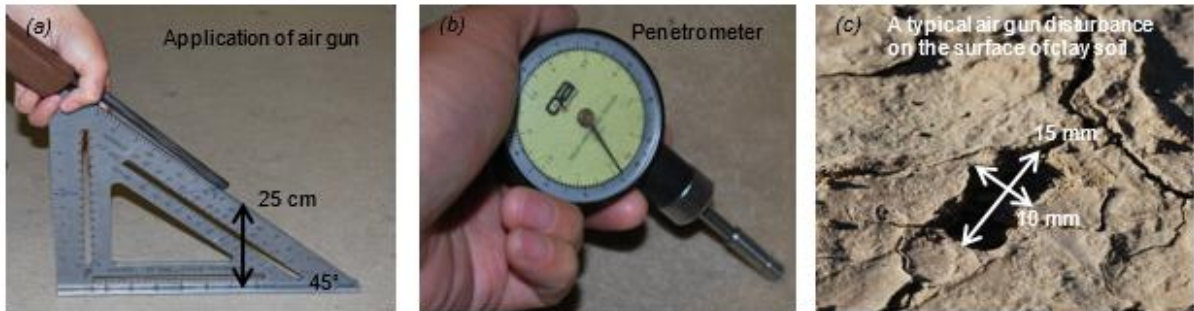


Figure 9. (a) A 4.5 mm diameter copper sphere is fired at 45° approximately 25 cm from the soil surface. (b) A penetrometer is applied to the soil surface at a 45° angle to gauge the surface resistance to disturbance. (c) This is the typical shape of a disturbance created by the air gun. The long and short diameter are measured and used to calculate the disturbance area.

#### 4.4 Soil Analysis

Prior to REE application the soil from each microsite type, shrub, grass, and bare, was assessed for its mineralogy, background concentration of REEs, and its grain size distribution. The mineralogy analysis was carried out using X-Ray diffraction (XRD) methods. The samples were ground to less than 2  $\mu\text{m}$  using a mortar and pestle then run through the XRD (Bruker D8 Advance) with a  $2\theta$  range of 6-71°, a step size of 0.02°, and a step time of 76.80 s. The particle size analysis was conducted using a Beckman Coulter LS 13 320 laser diffraction particle size analyzer and the background REE concentrations were obtained using Inductively Coupled Plasma Optical Emissions Spectrometry (ICP-OES) (Thermo Scientific™ iCAP™ 7200 Series). To prepare samples for ICP analysis

samples were partly digested using the US EPA Method 3051 A (US EPA, 2007) in a microwave digester (CEM Mars 6 – Microwave Digestion System).

#### 4.5 Rare Earth Element Tracers

For this study, we implement the REE application protocols for wind erosion developed by *Van Pelt et al.* (2012, 2014, 2017b). Holmium oxide ( $\text{Ho}_2\text{O}_3$ ), Ytterbium oxide ( $\text{Yb}_2\text{O}_3$ ), and Europium oxide ( $\text{Eu}_2\text{O}_3$ ) were applied on shrub, bare, and grass microsites respectively. The choice of REE oxides was determined by their low background concentrations in the soil, availability, and price. A calculated mass of each REE oxide was dissolved in nitric acid (3 N), diluted with deionized water, and then sprayed onto microsites using a calibrated sprayer to insure a uniform concentration (*Van Pelt et al.*, 2012, 2014). The volume sprayed was calculated using the area of each microsite in order for the tracer to penetrate the top 2 cm of the soil profile (*Van Pelt et al.*, 2014). The spiked target concentration was 500 times that of the background concentration.

To determine the background and spiked REE tracer concentrations, 50 randomly distributed samples (10 g each) were taken from the top 2 cm of soil in each (5×5 m) sampling area before REE application at the beginning of the windy season (March) and after REE oxide application. Samples were taken from the surface of bare microsites and from the pedestal of shrub and grass microsites. Sediment samples were collected 90 days later after the windy season (June), to assess the depletion and enrichment of REEs at the different microsites. The Kruskal-Wallis statistical test (NCSS 11, 2016) was conducted

for each REE tracer in each microsite type. This test compared the spiked time zero concentrations to the burned and the control plot concentrations 90 days later.

A minimum of 15 samples from each of the three replicated plots (post-windy season) within the two treatment areas (burned and control) were analyzed for the concentration of REEs. Of the analyzed burned treatment samples 32 were from bare sites, 15 were from grass, and 16 were from shrub microsites. From the control area 57 bare, 14 grass, and 10 shrub samples were analyzed. Due to the limited mass of sediment (2g needed) collected by the control area MWACs 4 samples were analyzed whereas a total of 8 samples were analyzed from the burned area MWACs.

REE concentrations were measured using ICP-OES (Thermo Scientific™ iCAP™ 7200 Series). For this analysis, REEs were leached from the sand and silt-size fraction of soil samples using microwave digestion in concentrated HNO<sub>3</sub>-HCl (3:1) solution following the US EPA Method 3051A (US EPA, 2007). Soil samples (2.0 g) were placed in microwave digestion tubes followed by 9 mL trace-metal-grade concentrated HNO<sub>3</sub> and 3 mL concentrated HCl. The samples were allowed to predigest overnight. The microwave digestion process was conducted at 175°C for 30 minutes then cooled to room temperature. The digested samples were filtered through No. 5 Whatman filter papers and vacuum filtered through 0.45 µm membranes. The filtered samples were diluted to 50 mL for ICP-OES analysis.

In order to create ternary mixing diagrams, the background REE concentrations were subtracted from the sample REE concentrations and normalized to the average spiked concentration minus the background. Individual normalized sample concentrations were

then divided by the sum of all normalized concentrations, yielding the percent of each REE component.

$$(C_{Si} - C_{Bi}) / (C_{Ai} - C_{Bi}) \quad (8)$$

$$\frac{(C_{Si} - C_{Bi}) / (C_{Ai} - C_{Bi})}{\sum \left( \frac{C_{Si} - C_{Bi}}{C_{Ai} - C_{Bi}} \right)} \quad (9)$$

where  $C_{Si}$  is the concentration of the  $i^{\text{th}}$  tracer in sediment samples,  $C_{Bi}$  is the background concentration of the  $i^{\text{th}}$  tracer, and  $C_{Ai}$  is the initial spiked concentration of the  $i^{\text{th}}$  tracer applied to the soil surface.

## CHAPTER 5: RESULTS

Grain-size analysis using the laser diffraction particle size analyzer showed variations in grainsize between each microsite type (Table 1). When sieved, excluding particles greater than 2 mm, the bare sites (9.93% clay, 30.24% silt, and 59.82% sand) contained the greatest portion of fine sediment, whereas shrub sites (3.38% clay, 17.21% silt, and 79.40% sand) contained the coarsest. The particle size distributions appear to be bimodal for all three cover types with bare site peaks at 101 and 510  $\mu\text{m}$ , grass peaks at 105 and 525  $\mu\text{m}$ , and shrub peaks at 128 and 624  $\mu\text{m}$  (Figure 10). Thus, both bimodal peaks become coarser from bare to shrub sites. Bare sites contained more gravel than the other sites. XRD analysis reveals that the soil is primarily made up of quartz, orthoclase, albite, and calcite (Figure 11).

Table 1. The percent distribution of particle sizes within the three different micro sites.

	Average Clay %	Average Silt %	Average Sand %
Bare	9.93	30.24	59.82
Grass	4.16	23.08	72.75
Shrub	3.38	17.22	79.40

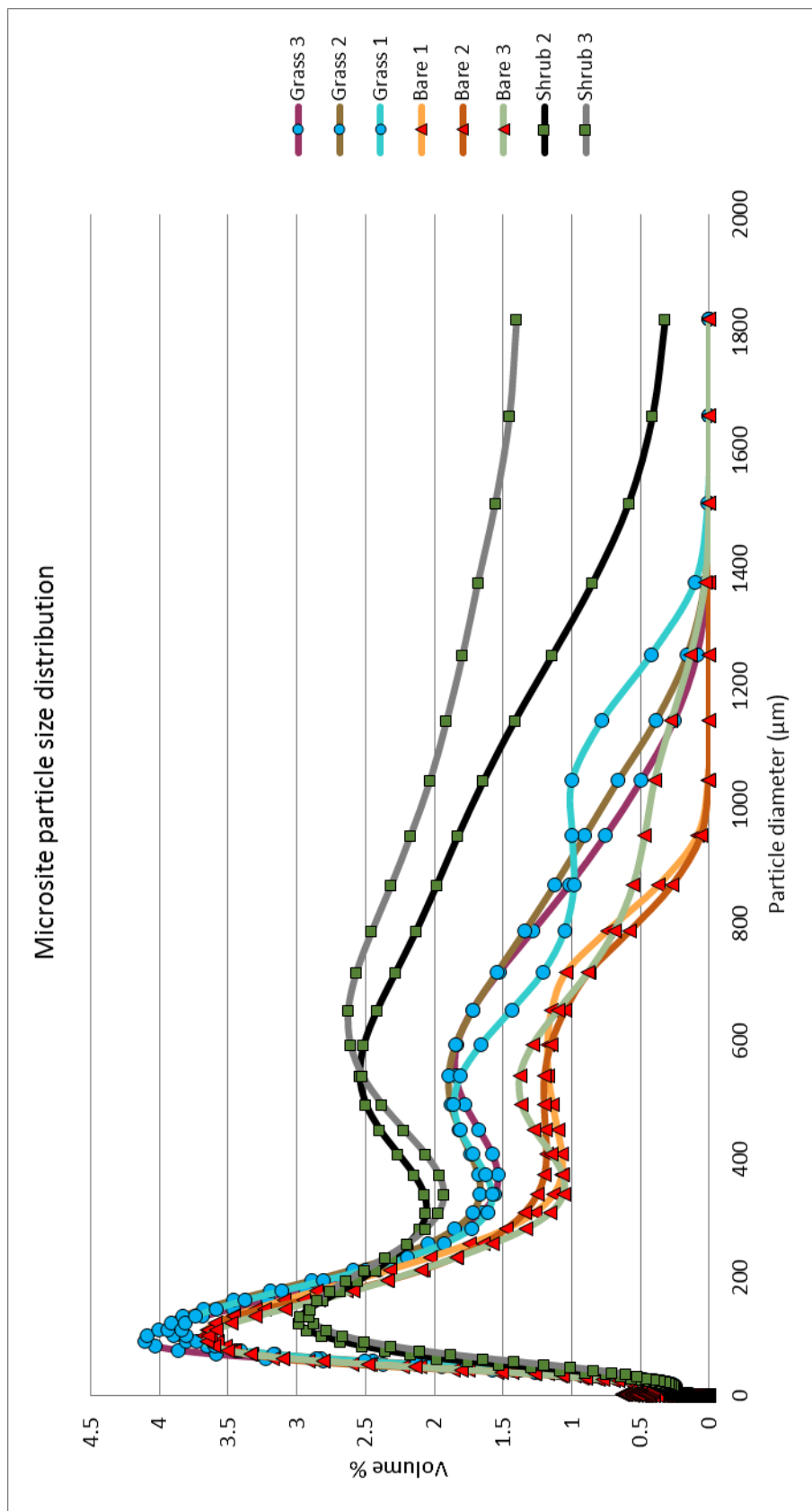


Figure 10. The particle size distribution for the three different microsite types. Grasses are denoted by the blue circles, bare sites by the red triangles, and the shrub sites by the green squares. Each cover type displays a bimodal distribution which coarsens from bare sites to grass sites to shrub sites.

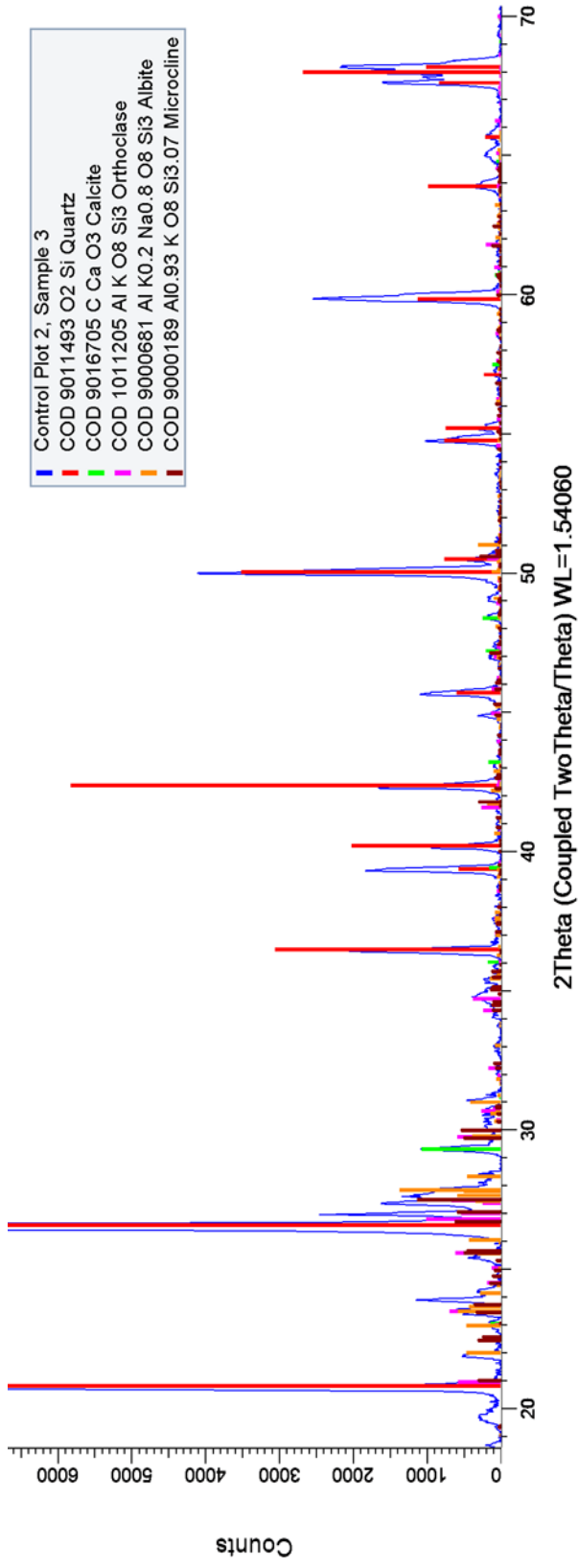


Figure 11. X-ray powder diffractogram of a Sevilletta soil sample made up of quartz, orthoclase, and calcite.

Using the Kruskal-Wallis test with a 95% confidence limit, the average daily soil volumetric water content (VWC,  $\text{m}^3 \text{m}^{-3}$ ) shows significant differences between microsites in both the burned and control treatment areas (Figure 12). Bare microsites in both treatment types have VWCs that are not significantly different. However, in both cases, burned and control, bare microsites differ from the vegetated site, shrub and grass. Burned grasses have the highest VWC of their treatment type whereas the control plot grasses have the lowest VWC with control grass VWCs lower than that of the burned. Burned grasses are not significantly different than control shrubs. Burned shrubs have the lowest overall VWC with a mean close to zero. The shrub sites in the control plot have the highest of all the VWCs.

The trends in VWC through time (averaged over 1 min) differ between the burned plot and the control (Figures 13 and 14). Five peaks showing increases in the VWC are associated with precipitation events on 4/8/16 (6.60 mm), 4/12/16 (4.06 mm), 5/1/16 (1.02 mm), 5/18/16 (7.62 mm), and 5/31/16 (0.25 mm) (Figures 13 and 14). VWC decreases during the day and increases at night, resulting the small scale saw-tooth pattern in figures 13 and 14. The control plot grass and bare site VWC reacts similarly to precipitation showing a sharp increase following the event and a subsequent gradual decline. Shrubs, however, exhibit a distinct lag in the maximum VWC following precipitation events and a gradual decline in soil moisture. The control grass VWC is always less than that of the bare. Contrasting with the control area, burned plot grasses have the highest VWC above that of the bare, though their peaks show similar trends. Burned shrub sites have the lowest VWC, often at zero. The VWC lag, which was observed in control shrubs is no longer

present following the fire. Furthermore, burned shrubs never reach the same VWC as grass or bare spaces even following precipitation events.

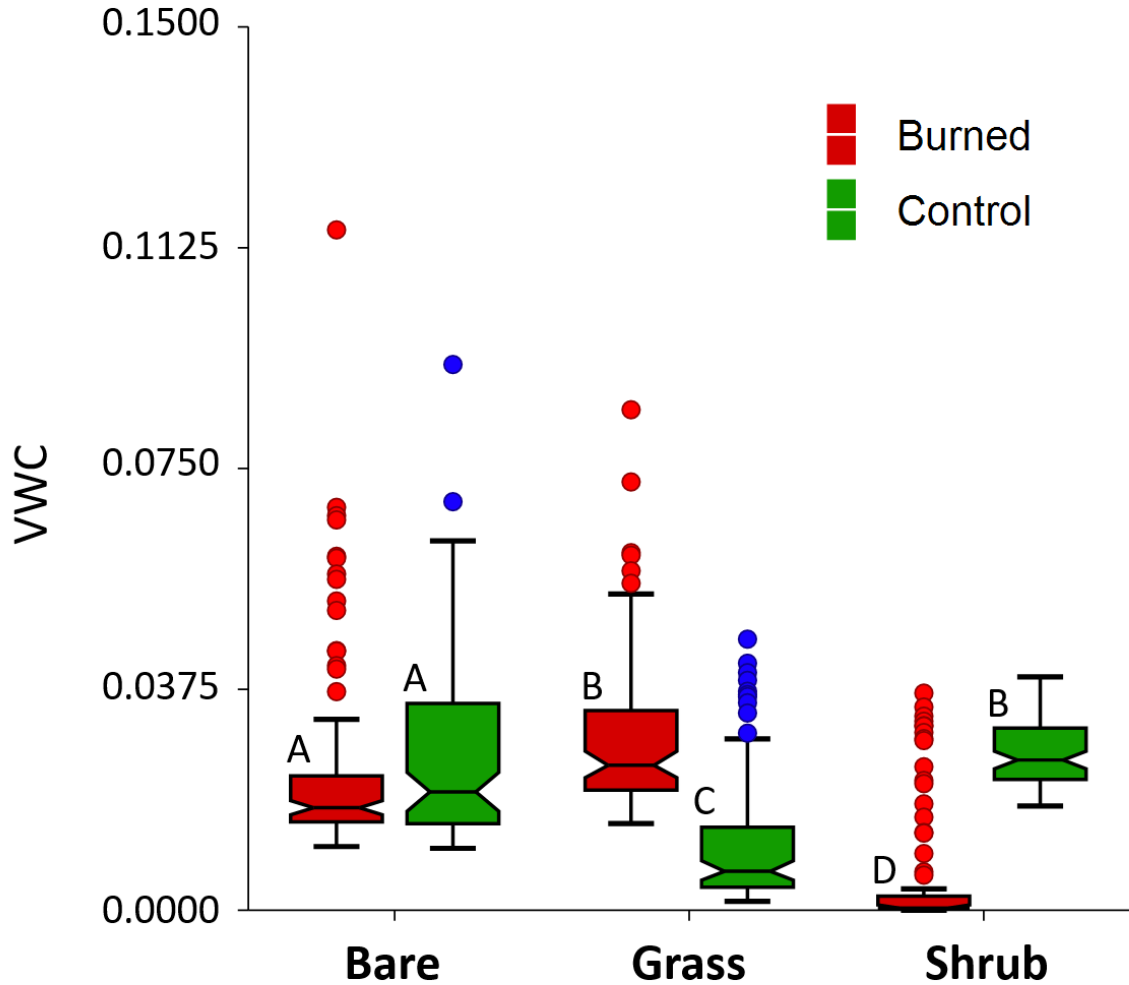


Figure 12. Notched box plots of VWC from the burned (red) and the control (green) Outliers are represented with red (burned) and blue (control) dots. Significant differences were established through the Kruskal-Wallis test with a 95% confidence limit. Significantly different groups are denoted with the alphabetical symbols A, B, C, and D.

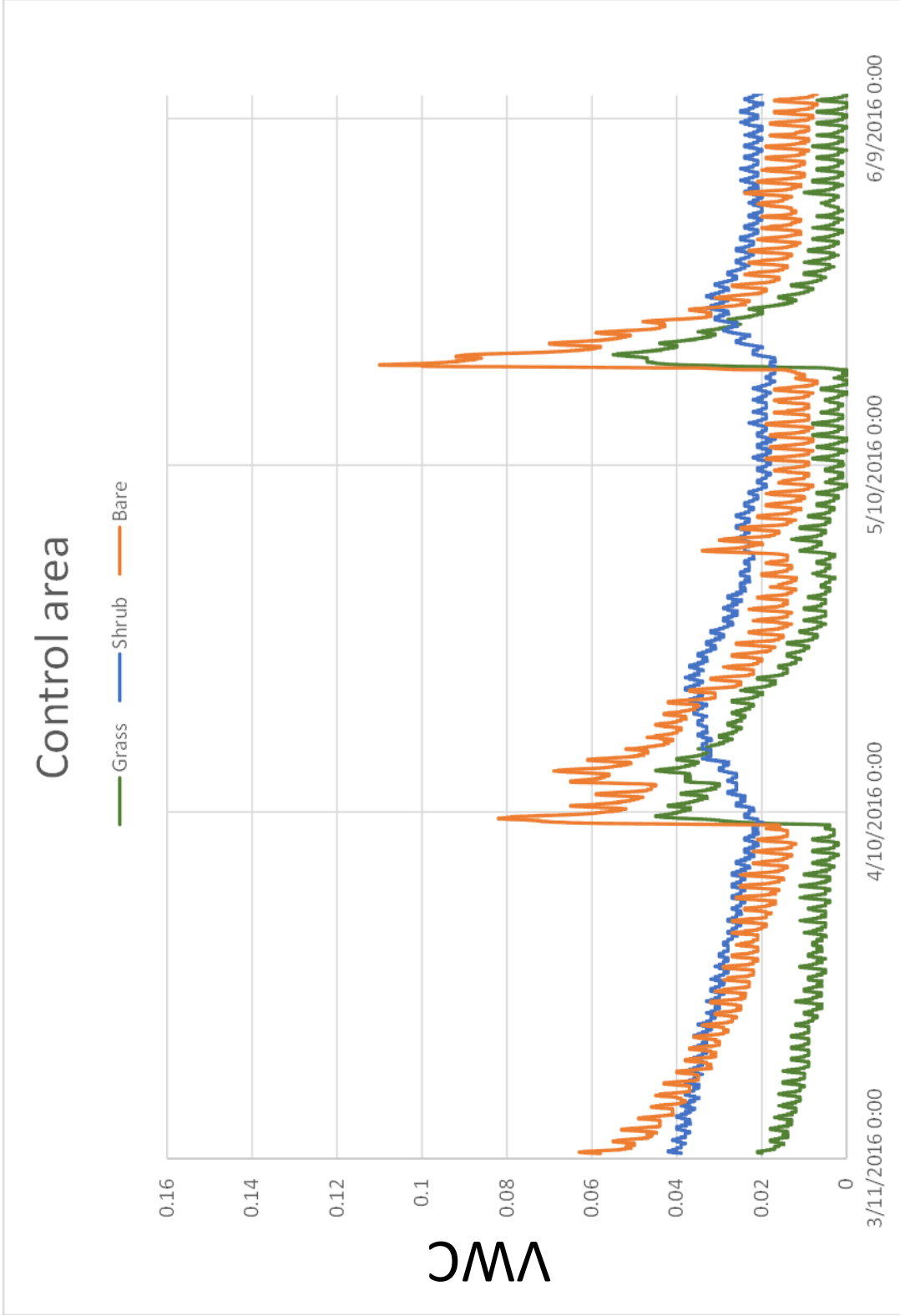


Figure 13. The VWC of the control plot through time (90 day of the windy season) averaged over 1 min intervals. Bare sites are in orange, grass sites in green and shrub sites are in blue. The large increases in VWC are precipitation events. The small oscillations in VWC are diel variations.

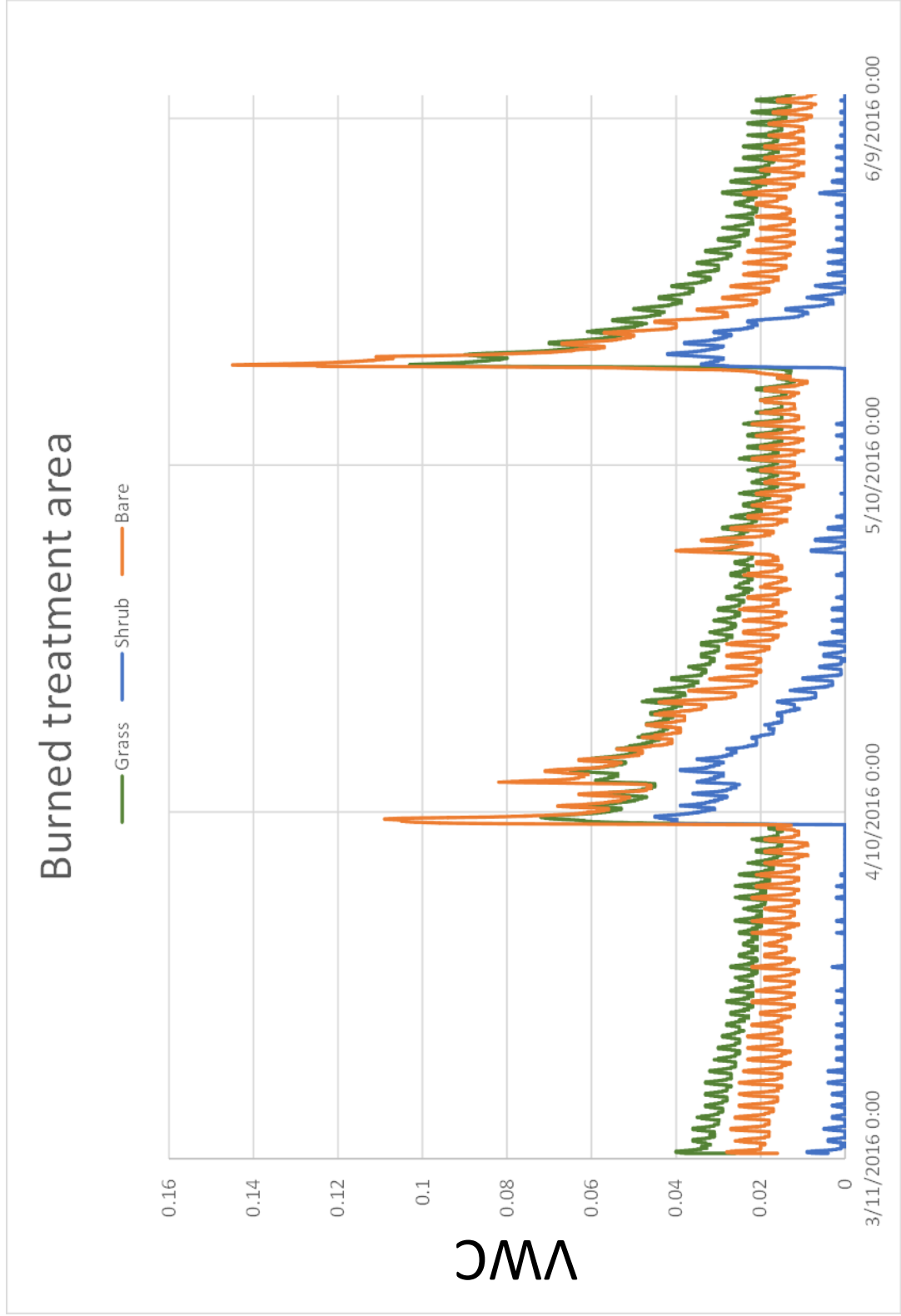


Figure 14. The VWC of the burned area varies with time (90 days of the windy season) averaged over 1 min intervals. The orange line represents the bare site, green is the grass site, and blue is the shrub site. Large increases in VWC are precipitation events. Small oscillations in VWC are diel variations.

The wind velocity observed at four different heights in both treatment areas decreases as it approaches the soil surface (Figure 15). The wind velocities for the burned area are higher than that of the control at a height  $\leq 0.5$  m. The difference in wind speed between the two treatment areas (burned > control) becomes significant (using the Kruskal-Wallis test with a 95% confidence limit) closer to the soil surface indicating that the shear velocity at the soil surface must be higher in the burned area than it is in the control. When the daily surface shear velocity of the wind was modeled between the two treatment types the burned surface shear ( $0.2947 \pm 0.0694 \text{ m s}^{-1}$ ) was significantly greater (t-test, 95% confidence limit) than that of the control area ( $0.1683 \pm 0.0433 \text{ m s}^{-1}$ ) (Figure 16).

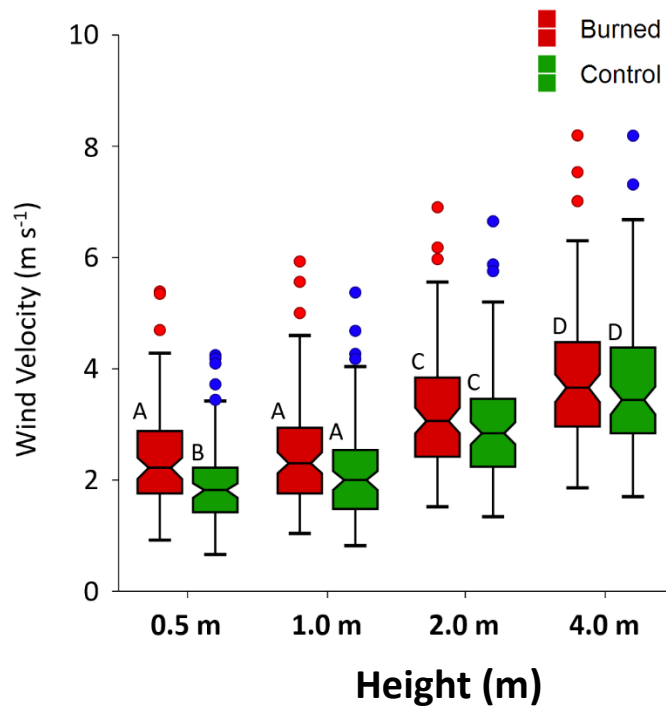


Figure 15. Notched box plots show the daily average wind speed at varying heights in the burned and control areas over a period of 90 days. The burned areas are denoted in red while the control are denoted in green. The blue and red points represent outliers and the letters A, B, C, and D show significant and no significant difference. Burned area wind speeds are consistently greater than control area wind speeds. The difference becomes significant at 0.5 m.

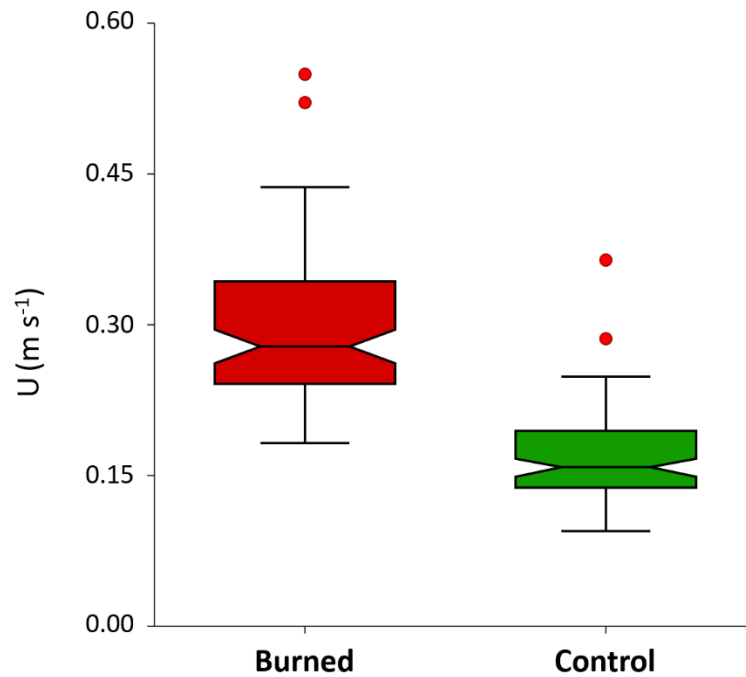


Figure 16. Notched box plots of the surface wind shear ( $U$ ) in both the burned and the control plot. Both were found to differ significantly using a T-test with a 95% confidence limit. The red points represent outliers.

The average total HMF ( $Q$ ) in the control and burned plots were  $27.1 \pm 2.4$  and  $75.3 \pm 55.0 \text{ gm}^{-1}\text{d}^{-1}$  respectively (Figure 17a). The burned plot average was approximately three times greater than that of the control plot. Kruskal-Wallis One-way ANOVA on Ranks results indicate that the average total HMF was significantly different between the control and burned plots ( $p < 0.05$ ) (Figure 17a). The  $k$  constant used to determine the VDF was found to be  $4.07 \cdot 10^{-4} \pm 8.23 \cdot 10^{-5} \text{ m}^{-1}$ . The VDF ( $F_e$ ), propagating the uncertainty, was found to be  $1.10 \cdot 10^{-2} \pm 2.43 \cdot 10^{-3}$  and  $3.07 \cdot 10^{-2} \pm 2.33 \cdot 10^{-2} \text{ gm}^{-2}\text{d}^{-1}$  for the control and bare respectively (Table 2). The VDF also increases approximately three times.

The TSVs ( $u_t$ ) estimated from the surface resistance indicate that the microsities differed significantly between the shrub ( $0.40 \pm 0.13 \text{ m s}^{-1}$ ), grass ( $0.61 \pm 0.11 \text{ m s}^{-1}$ ), and

bare soil ( $0.63 \pm 0.11 \text{ m s}^{-1}$ ) microsites based on One-way ANOVA ( $F=22.96, p<0.001$ ) (Figure 17b, Table 3). The TSV ( $u_t$ ) values decreased significantly after the prescribed fire for the shrub ( $0.20 \pm 0.08 \text{ m s}^{-1}$ ) and grass ( $0.41 \pm 0.14 \text{ m s}^{-1}$ ) microsites, and remain unchanged for bare ( $0.62 \pm 0.08 \text{ m s}^{-1}$ ) soil based on the Kruskal-Wallis Multiple-Comparison Z-Value Test at a 95% confidence limit (Figure 17b).

Table 2. The horizontal mass flux from both the treatment areas (burned and control) as well as the vertical dust flux derived from the percent clay content in the soil.

	HMF ( $\text{gm}^{-1}\text{d}^{-1}$ )	VDF ( $\text{gm}^{-2}\text{d}^{-1}$ )
Control	$27.1 \pm 2.4$	$1.10*10^{-2} \pm 2.43*10^{-3}$
Burned	$75.3 \pm 55$	$3.07*10^{-2} \pm 2.33*10^{-2}$

Table 3. Calculated threshold shear velocity of the soil surface under each microsite type obtained using an air rifle method. The values are averaged to show the mean TSV, the standard deviation and coefficient of variation is also presented.

TSV(m/s) Trial	Burned shrub	Burned grass	Burned bare	Control shrub	Control grass	Control bare
1	0.20	0.27	0.66	0.17	0.47	0.66
2	0.19	0.20	0.62	0.40	0.66	0.71
3	0.19	0.30	0.69	0.48	0.66	0.63
4	0.20	0.61	0.43	0.47	0.73	0.72
5	0.14	0.61	0.63	0.40	0.54	0.71
6	0.23	0.40	0.51	0.55	*	0.75
7	0.19	0.36	0.66	0.43	*	0.65
8	0.13	0.45	0.66	0.19	*	0.43
9	0.40	0.54	0.66	0.40	*	0.45
10	0.15	0.34	0.66	0.51	*	0.61
mean	0.20	0.41	0.62	0.40	0.61	0.63
stdev	0.08	0.14	0.08	0.13	0.11	0.11
c.v.	0.38	0.35	0.13	0.32	0.17	0.17

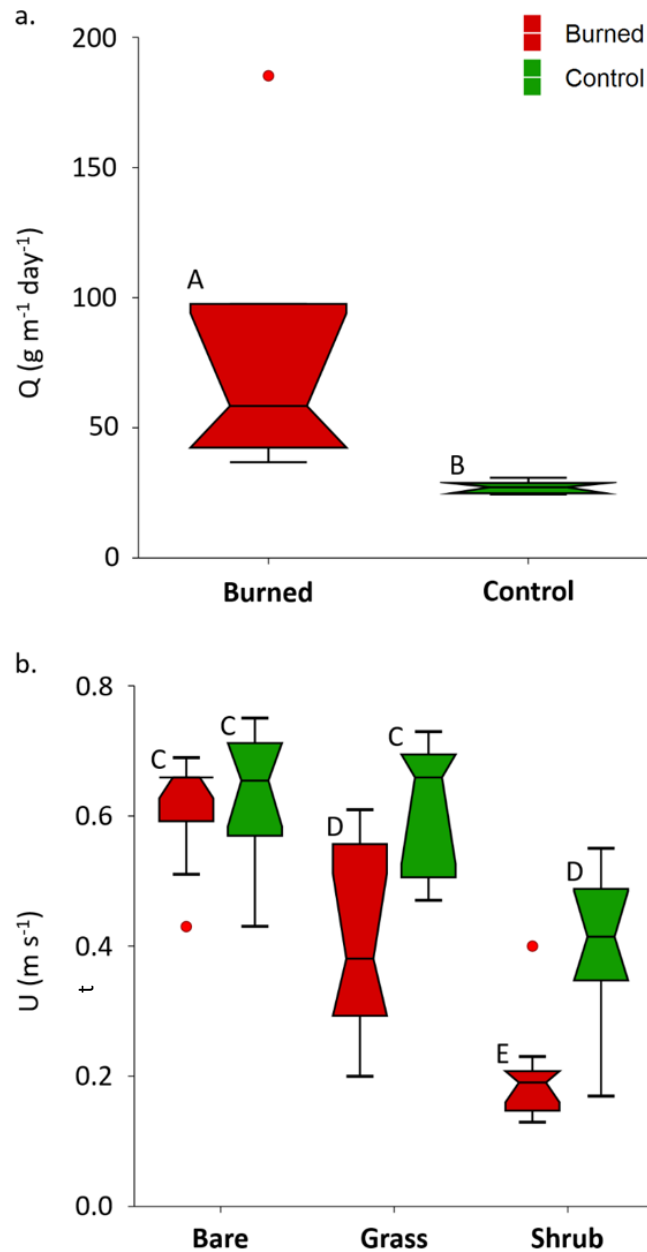


Figure 17. (a) The derived total HMF ( $Q$ ) from MWAC sediment samplers in the control and burned plots show an average of  $27.1 \pm 2.4$  and  $75.3 \pm 55.0 \text{ g m}^{-1} \text{day}^{-1}$  respectively. The control and burned flux are significantly different as shown by the box plots and the Kruskal-Wallis One-Way ANOVA on Ranks statistical test. Significant difference is denoted by the A and B symbols. The red point represents an outlier. (b) The TSV ( $u_i$ ) of bare, grass, and shrub sites was derived using measured surface resistances. Grass and shrub TSVs ( $u_i^*$ ) decreased significantly following fire and bare sites remained constant as shown by Kruskal-Wallis Multiple Comparison Z-Value test at a 95% confidence limit. Significant differences are indicated by the differing symbols, C, D, and E. Red points are outliers assuming a normal distribution.

The background concentrations of individual REEs range from 15.4 to 0.272 ppm (Table 18). The Oddo-Harkins effect, where even atomic number elements are more abundant than odd, can be seen in the heavy REEs (Figure 18). Our original goal was to spike the concentration of REE in the soil approximately 500 times that of the background concentration. Because the lighter REEs such as La and Ce, are more abundant than the heavier REEs, selected heavy REEs as tracers for our study. Eu, Yb, and Ho were chosen because of their low concentration and relatively low price. When the REEs were applied to the soil the spiked concentrations reached over 100 times the background concentration (Figure 19).

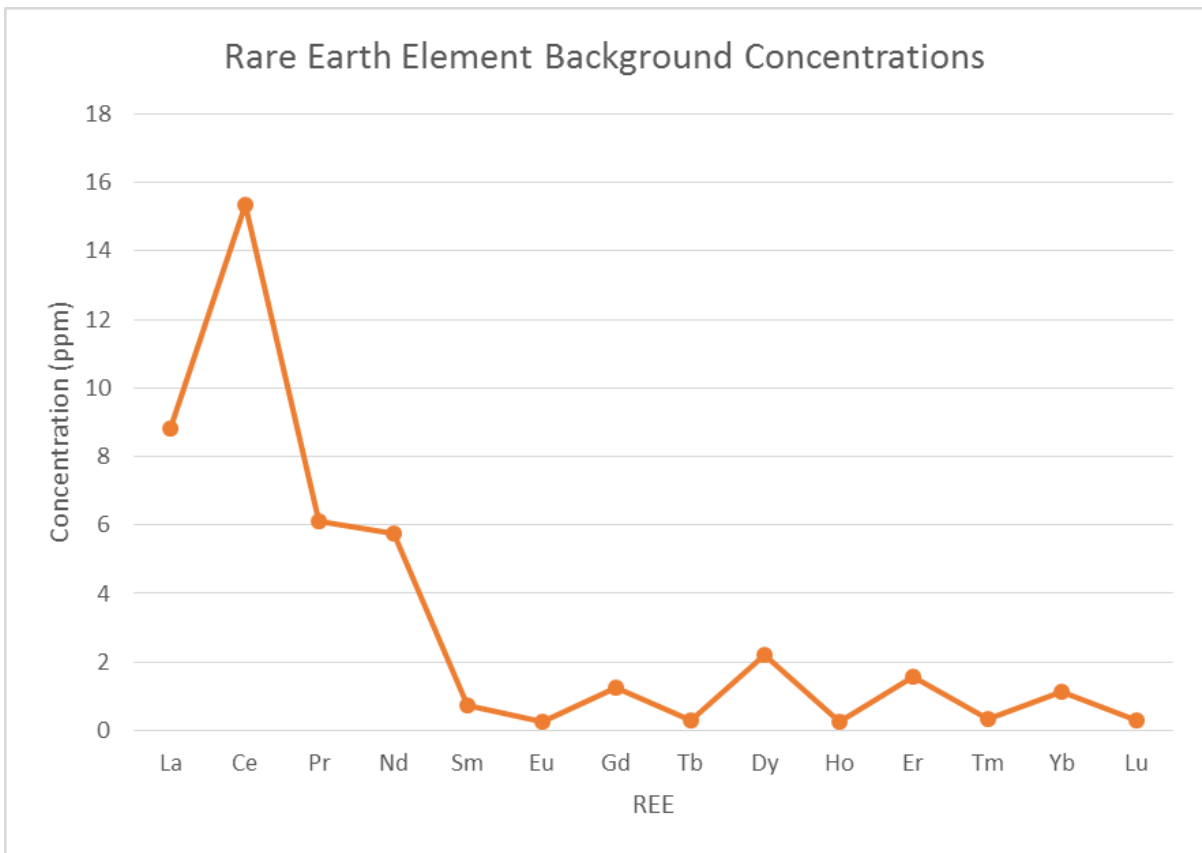


Figure 18. The mean background concentration of REEs in the soil for each microsite type. The light REEs are much more abundant than the heavier REEs. Eu, Ho, and Yb were chosen as tracers because of this.

Table 4. The average background concentrations of REEs in Sevilleta soil.

REE	Background Concentration (ppm)
La	8.825131312
Ce	15.35877843
Pr	6.104515156
Nd	5.749543425
Sm	0.748535919
Eu	0.256657441
Gd	1.240983522
Tb	0.280972857
Dy	2.20453374
Ho	0.271828221
Er	1.577826809
Tm	0.316033166
Yb	1.12547965
Lu	0.277695135

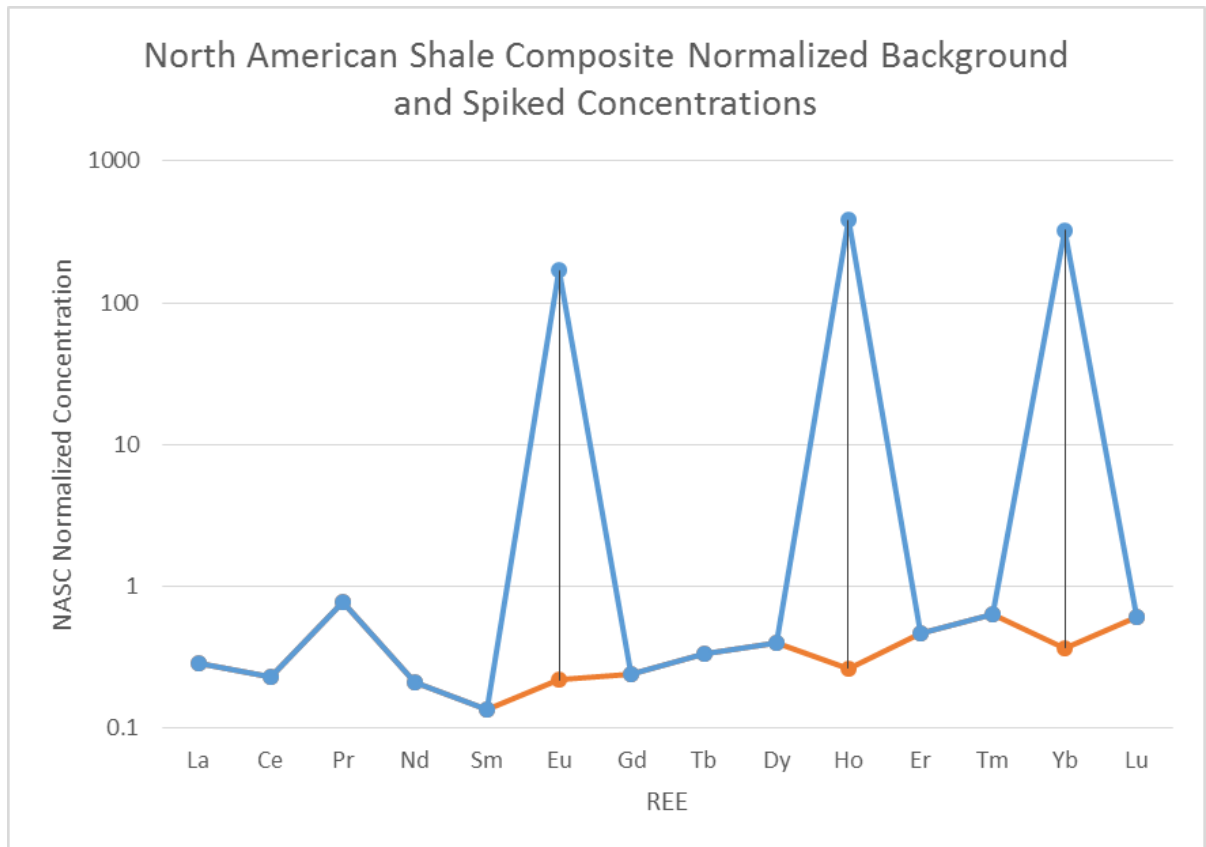


Figure 19. The shale normalized (NASC) spiked REE concentrations as well as the background REE concentrations (*Gromet et al.*,1984). The graph is plotted on a log scale. Each of the spiked REEs is greater than 100 times the background concentration.

After the windy season, the proportions of the REEs differed greatly between the control and the burned plots (Figures 20 and 21). Control plots exhibited a mixture of tracers from bare sites in the vegetated microsites (shrub and grass) (Figure 20); both grass and shrub microsites were enriched with Yb, the tracer initially applied on the bare interspaces. The sediments from the MWAC samplers in the control area plots contained high proportions of the bare microsite tracer (Yb; mean =  $88.5 \pm 1.7\%$ ), compared to those in the burned area plots (Yb; mean =  $39.1 \pm 9.3\%$ ) (Figures 20 and 21). In the control plots, there was no significant enrichment of bare sites with tracers initially applied to the vegetated sites (ie., Ho and Eu) and no exchange of Ho and Eu tracers occurred between the shrub and grass microsites (Figures 22, 23, 24). The burned site showed more mixing

than the control, suggesting interaction between all three microsite types (Figure 21). The sediments from the MWAC samplers in the burned area showed a mixture between shrub (Ho) and bare (Yb) microsite tracers,  $42.3 \pm 13.8\%$  and  $39.1 \pm 9.3\%$  respectively. Grass microsites were more enriched with shrub tracer than vice versa (Figure 25).

The bare tracer (Yb) in the bare microsites showed no significant difference between the spiked, control, and burned plots at the 95% confidence level (Figure 22a), whereas the REE tracers applied under vegetation, Eu and Ho, in bare microsites experienced a significant increase in the burned plots compared to the spiked and the control (Figures 22b, 22c). The grass microsites demonstrated: a significant increase in Yb tracer, applied to bare interspaces initially, in both the control and burned plots (Figure 23a); no significant grass tracer (Eu) difference between the spiked, control, and burned plots (Figure 23b); and a significant increase in shrub tracer (Ho) in burned plots compared to the control and spiked concentrations (Figure 23c). Shrub microsites followed a similar pattern to the grasses with a significant increase in bare tracer (Yb) concentrations in both the burned and the control plots (Figure 24a). In addition, a significant increase in grass tracer (Eu) in the shrub sites of the burned plot was observed (Figure 24b), but no significant difference existed in the concentration of shrub tracer (Ho) in shrub sites (Figure 24c).

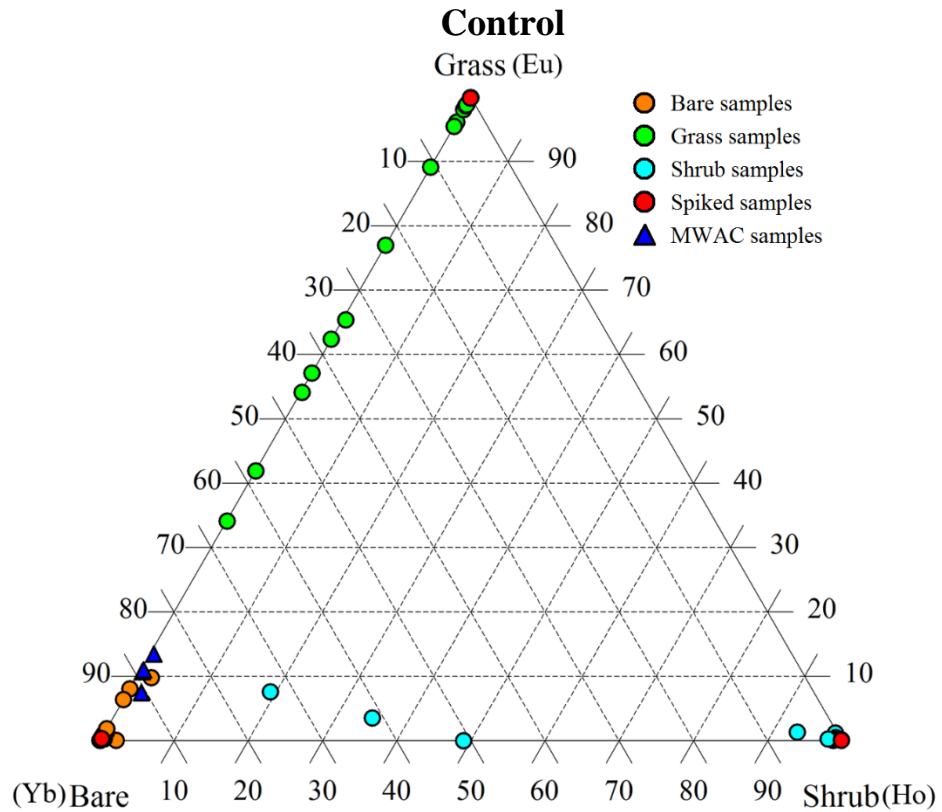


Figure 20. A ternary plot of control area weight percent element composition normalized to the spiked REE concentrations (equation 9) shows mixing between three end members; bare (Yb), grass (Eu), and shrub (Ho). Red dots at or near the vertices indicate that the initial spiked concentrations of these REE are more than 100 times background values at time zero. Orange dots display the composition of bare samples after 90 days, green dots are grass samples (90 days), light blue dots are shrub samples (90 days), and the dark blue triangles show the composition of sediment taken from the MWAC samplers. The data points which plot along or near the bare-shrub and bare-grass axes and the dark blue triangles which plot in the bare corner indicate that the main sediment source is from bare patches and there is limited sediment mixing between the shrub and grass sites.

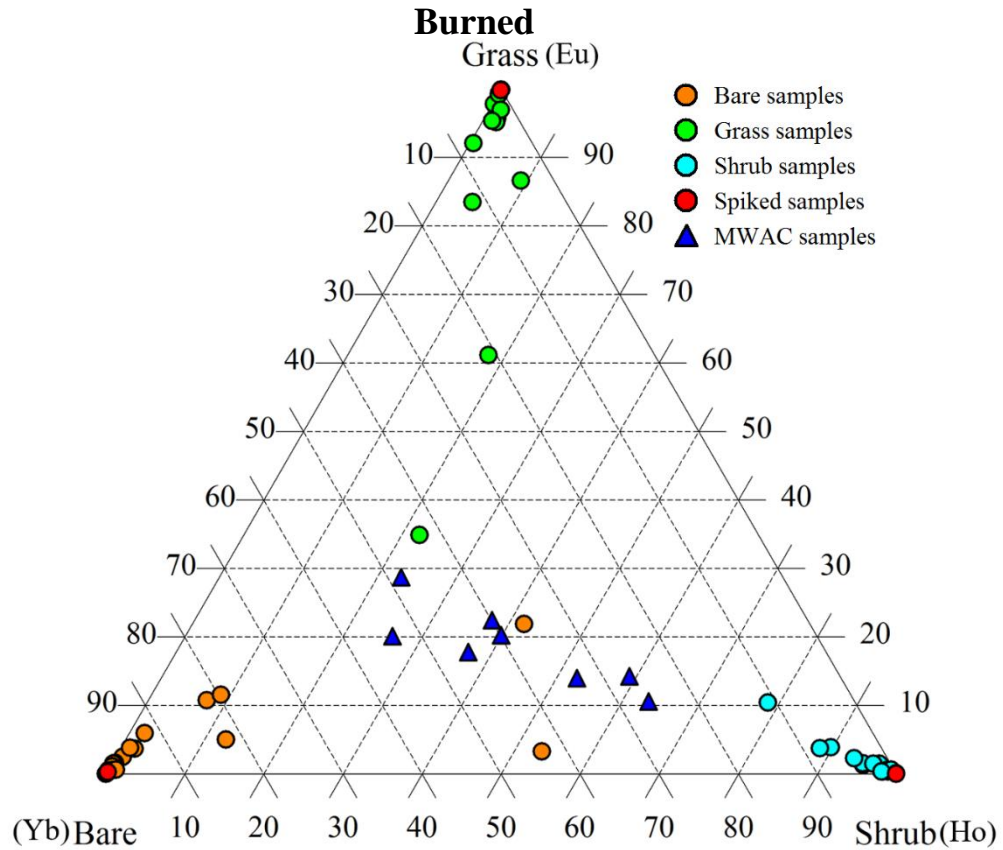


Figure 21. A ternary plot of burned area weight percent element composition normalized to the spiked REE concentrations (equation 9) shows mixing between three end members; bare (Yb), grass (Eu), and shrub (Ho). Red dots at or near the vertices indicate that the initial spiked concentrations of these REE are more than 100 times background values at time zero. Orange dots display the composition of bare samples after 90 days, green dots are grass samples (90 days), light blue dots are shrub samples (90 days), and the dark blue triangles show the composition of sediment taken from the MWAC samplers. Green and light blue data points plot farther away from the bare-shrub and bare-grass axes and the dark blue triangles plot predominantly along the bare-shrub axis indicating that the main sediment source is from the bare and shrub patches and that there is mixing between all three microsite types.

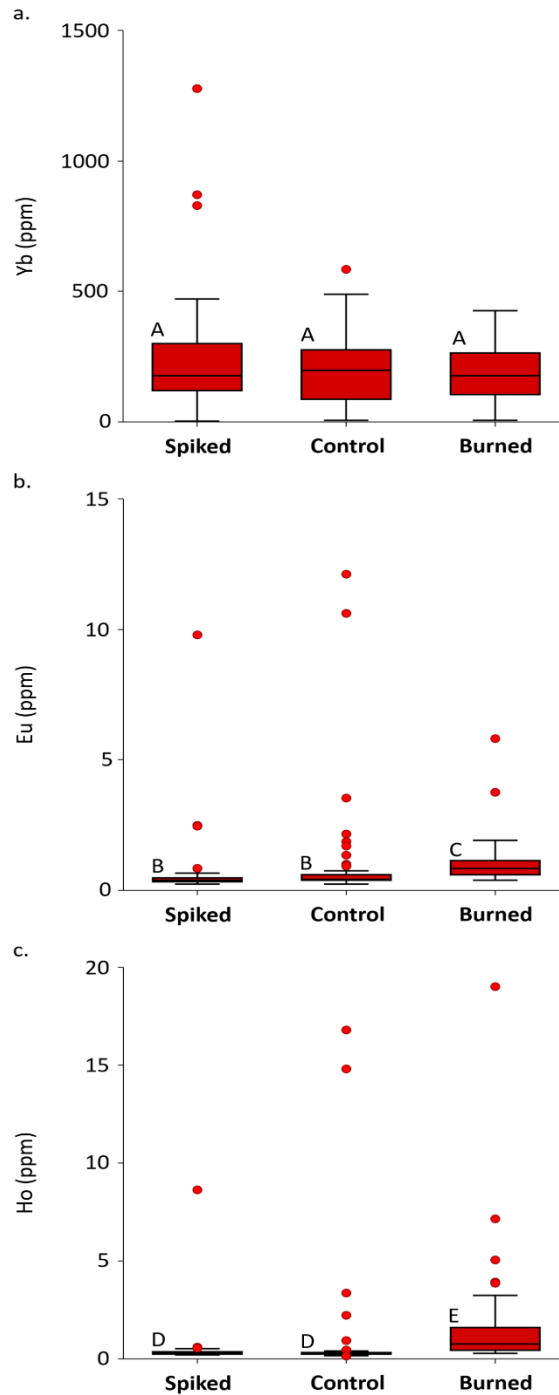


Figure 22. Box plots compare tracer REE concentrations in bare microsites between spiked, control and burned plots. Red points are outliers assuming a normal distribution. (a) Bare tracer (Yb) concentrations are not significantly different ( $P > 0.05$ ) in the three sites as indicated by the A symbol. (b) The grass tracer (Eu) concentrations are significantly greater in the burned site than in the control and original spiked plot as indicated by the C symbol. (c) The shrub tracer (Ho) concentration is also significantly greater in the in the burned plot than in the control and original spiked plot as indicated by the E symbol.

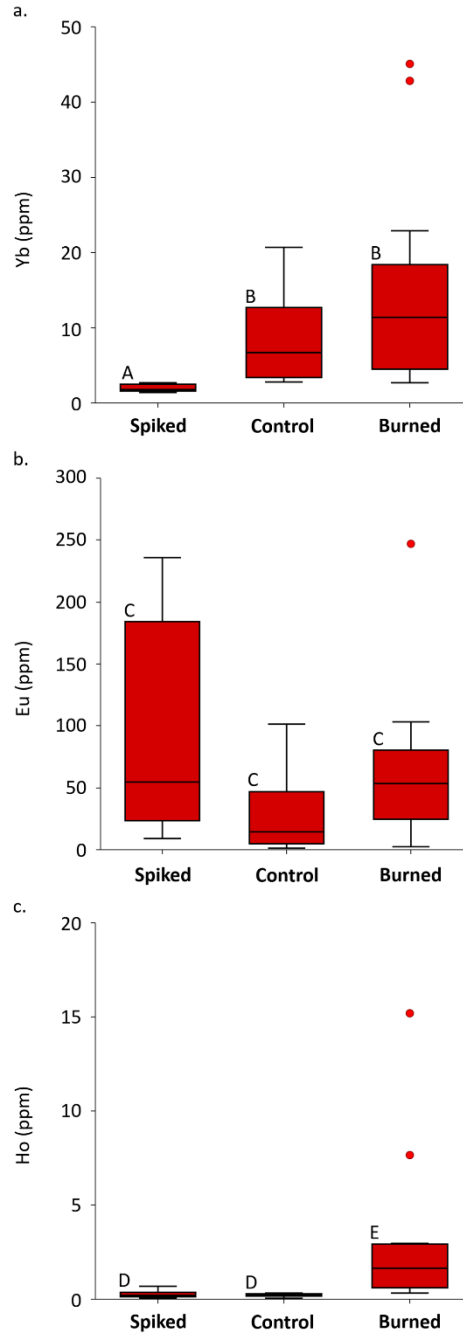


Figure 23. Box plots compare tracer REE concentrations in grass microsites between spiked, control and burned plots. Red points are outliers assuming a normal distribution. (a) Bare tracer (Yb) concentrations in grass sites are significantly greater in the burned and control plots than the spiked as indicated by the B symbol. (b) The grass tracer (Eu) concentrations are not significantly different ( $P > 0.05$ ) in the three plots as indicated by the C symbol. (c) The shrub tracer (Ho) concentrations are significantly greater in the burned plot than the spiked and the control plots as indicated by the E symbol.

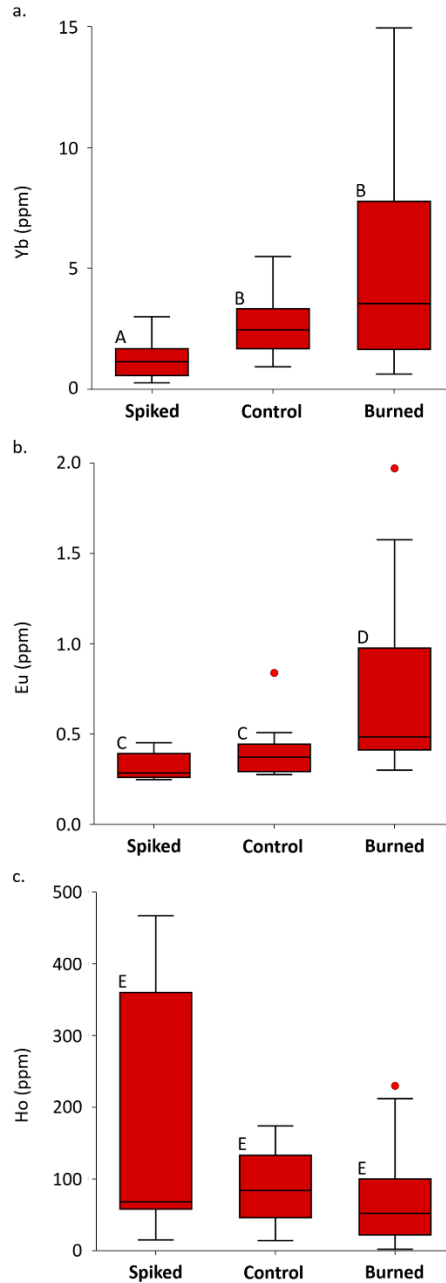


Figure 24. Box plots compare tracer REE concentrations in shrub microsites between spiked, control and burned plots. Red points are outliers assuming a normal distribution. (a) The bare tracer (Yb) concentrations in shrub sites are significantly greater in the burned and control plots than the spiked as indicated by the B symbol (b) The grass tracer (Eu) concentrations in shrub sites are significantly greater in the burned plot than in the spiked and the control plots as indicated by the D symbol. (c) The shrub tracer (Ho) concentration in the shrub sites is not significantly different ( $P > 0.05$ ) between all three plots as indicated by the E symbol.

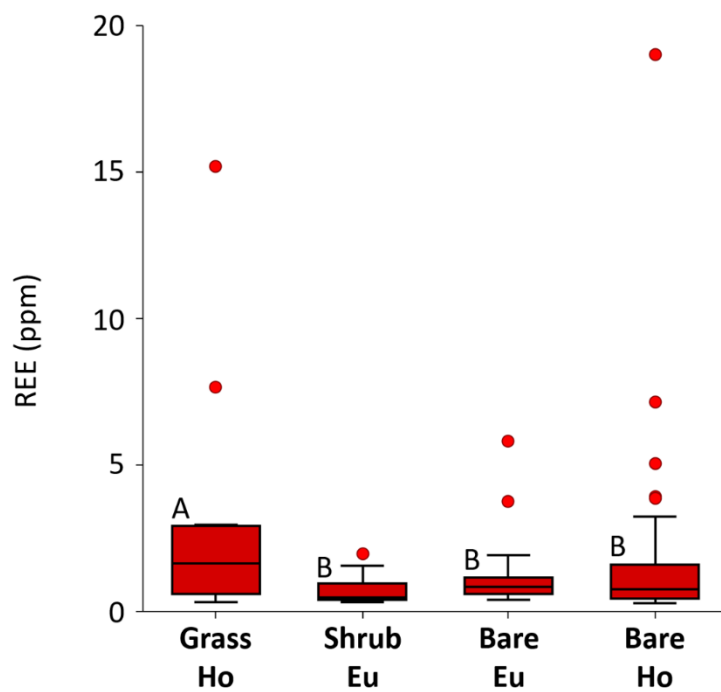


Figure 25. Box plots comparing vegetative tracer (Ho and Eu) concentrations in all three burned plot microsites. Based on the Kruskal-Wallis test, Ho concentrations in the grass site (A) are significantly greater than in the other sites (B). Red points are outliers assuming a normal distribution.

## CHAPTER 6: DISCUSSION

Field experiments in a shrub-grass transition zone in the Chihuahuan desert using wind erosion monitoring and rare earth element tracers indicate that fires greatly increased the transport and redistribution of sediment by wind. The HMF of wind-borne sediments were three times higher in the burned plots compared to the control plots (Figure 17a). The post-fire enhancement of aeolian processes is documented by several other studies and is attributed to the loss of vegetation cover and changes in surface soil properties (e.g., soil water repellency) in the burned sites (*Sankey et al.*, 2009; *Ravi et al.*, 2012). The HMF is the major process responsible for local redistribution of soil resources and typically more than 95% of the flux occurs below the measured 1-m height. As the vertical dust flux ( $F_e$ ) is linearly related to the HMF ( $F_e = kQ$ , where  $k$  is soil specific constant), it can be inferred that the vertical dust flux also increases three times in the burned areas (*Shao et al.*, 1993; *Gillette et al.*, 1997). If dust deposition in the system remains constant than the total erosion will also increase by three times the background.

Fires have a drastic effect on the VWC of the soil underneath the differing microsite types, potentially affecting the interparticle, stabilizing forces, which determine TSV (Figure 12). Shrub sites, which are characterized, in the control plot, by a broad and slow increase in VWC following precipitation events which occurred during the study period, show a change to a sharp but attenuated peak (~ half the height of bare and grass site peak VWC) following a similar pattern to the grass and the bare sites after the fire. Much of the time the burned shrub VWC is approximately zero which can be attributed to soil hydrophobicity often induced by the burning of woody vegetation (*DeBano*, 2000). Furthermore, the near zero VWC of burned shrubs due to soil hydrophobicity causes a

decrease in the interparticle forces (due to water retention) and results in a TSV decrease from  $0.40 \pm 0.13 \text{ m s}^{-1}$  to  $0.20 \pm 0.08 \text{ m s}^{-1}$  (Ravi *et al.*, 2006). The control grass sites have the lowest VWC for their treatment area, which can be attributed to interception of water by grasses and the uptake of soil water by grass roots. Following the fire grasses have the highest VWC, which may be due to lower evaporation relative to the bare sites and a decrease in transpiration relative to the control area. The comparably large VWC of grasses following fires may affect the TSV providing a feedback mechanism for the reestablishment of grasses during a woody plant invasion.

When measured, the TSV for each of the vegetated, shrub and grass sites, was significantly lower following the fire (Figure 17b). Both the grass and the shrub TSV decreased by approximately  $0.20 \text{ m s}^{-1}$ . The removal of vegetation as a roughness element and an associated decrease in VWC following the fire allows for an increase in the surface wind shear as well as a decrease in interparticle cohesive forces which results in greater erosion from shrub and grass sites. Shrub sites also have a lower TSV than that of grass sites. Thus, when vegetation is removed by fire, sediment is more easily (preferentially) entrained and transported from the shrub sites than it is from the grasses. This is supported by the REE concentrations found in the burned area sediment collectors (Figure 21).

The wind shear at the soil surface was greater in the burned plot than in the control (Figures 15 and 16). This is due to the removal of vegetation as a roughness element, which helps shelter the soil surface and decrease wind momentum (Stockton and Gillette, 1990). With a combination of decreased VWC due to soil hydrophobicity and the removal of the vegetation sheltering effect the TSV decreases over the soil surface following the fire. The increase in the wind shear velocity over this surface induces a HMF and VDF

approximately three times that of the background. Shrub sites have the lowest TSV and particles should be transported preferentially from these sites.

The REE-tracer analysis of wind-borne sediments showed that  $88.5 \pm 1.7\%$  of the HMF from the control area was derived from the bare microsites (Figure 20). The wind eroded sediments and nutrients are partially redeposited onto vegetated patches by canopy trapping. This deposition of fine soil and associated nutrients is thought to be the major factor responsible for the formation of shrub islands (*Schlesinger et al.*, 1990; *Li et al.*, 2008). Thus, the bare soil interspaces in shrub encroached landscapes that are not recently burned act as sediment sources while the vegetated microsites (shrub and grass) act as sinks for the sediments from bare soil sites. Because none of the data points are observed along or near the shrub-grass axis in Figure 20, the results show limited mixing of sediments between grass and the shrub microsites. Furthermore, no significant difference was observed between shrub and grass tracers (Ho and Eu) in bare sites indicating little to no erosion from vegetated microsites under stable (e.g., not recently burned) conditions (Figures 22, 23, 24).

The burned area displayed greater mixing of sediments occurring between all three microsite types compared to the control area (Figure 21). Significant enrichment of each microsite with tracers from the other two microsites (e.g., shrub and grass tracers in bare sites) indicates homogenization of sediment following the fire (Figures 22, 23, 24). The REE-tracer analysis of wind-borne sediments from the burned plots indicate that the HMF is primarily composed of particles from the bare and shrub microsites (Figure 21). These vegetated microsites were found to be the most active sediment sources following the fire, which corroborates experiments based on different methods in other burned desert

shrublands (*Sankey et al.*, 2012a). Greater enrichment of shrub tracers in grass microsites than vice versa indicates that the grass microsites became a significant sediment sink following the fire (Figure 25). The grasses are generally fire-adapted and typically retain their pedestals with dense fibrous roots which can stabilize the soil particles in grass microsites (*Stout*, 2012; *Van Pelt et al.*, 2017b). Moreover, the post-fire recovery of grasses is much faster than shrubs, thereby providing the grasses a competitive advantage in trapping aeolian sediments after a fire (*Parmenter*, 2008; *Ravi et al.*, 2009a).

The background characteristics of the soil showed that the bare sites contained the highest proportion of fine grains compared to that of the shrubs and the grasses with Shrub sites being the coarsest (Figure 10). The field site (shrub-grass transition zone) is in the early stages of shrub encroachment, which may account for the differences in grain size distribution between the microsite types. The greater amount of fine particles in bare sites may also explain their prominence as sediment sources in both the burned and control treatment areas. However, shrub sites are the dominant sediment source following the fire indicating that a decrease in soil moisture (VWC) and a removal of vegetation (sheltering effect) overcomes the difference in grain size between the bare microsite and the shrub microsites when determining the TSV of the soil. It is these mechanisms, which allow for the homogenization of the soil surface.

This study demonstrates that REEs can be used as effective and reliable tracers to identify post-fire sinks and sources of sediments at the field-scale. However, long-term field studies are needed to measure the different resource input and output components to accurately predict post-fire sediment redistribution and loss. *Zhang et al.* (2001) indicated that in sandy soils, REEs can be preferentially adsorbed to a certain fine fraction. Wind

preferentially entrains the smallest size fraction from the soil, which could lead to an overestimation or underestimation of erosion (*Li et al.*, 2009). However, in this study our objective was to compare the relative soil redistribution from the burned and unburned sites. Furthermore, we acknowledge that some disturbances to the surface soil may have inadvertently occurred in both the burned and control plots during the tracer application. Nevertheless, our study represents a useful approach to test the applicability of multiple REE tracers to quantify wind erosion and associated soil redistribution at field scales.

Our results support the post-fire resource redistribution and landscape homogenization hypothesized and tested by several studies (*White et al.*, 2006; *Ravi et al.*, 2009a; *Sankey et al.*, 2010, 2012b). Such homogenization can have undesirable environmental consequences in some desert shrublands, such as the cold desert sagebrush steppe of the Great Basin, USA (*Sankey et al.*, 2012b). However, in the shrub-encroached Chihuahuan desert grasslands that we studied in this experiment, the homogenization of resources and shrub mortality may enhance grass regrowth and competitiveness in the landscape, thereby proving a negative feedback to land degradation induced by shrub encroachment. Thus, prescribed fires could serve as a valuable management tool in the early stages of shrub encroachment when sufficient grass connectivity exists in the landscape for fires to spread. However, as observed in our study, fires can greatly accelerate the sediment transport by wind and subsequent dust emissions (Figure 17). Hence, the timing of fire and post-fire climatic conditions are important factors controlling the balance between resource loss and redistribution. For example, if the prescribed fires are followed by persistent droughts or extreme winds the ecosystem might experience a net loss of resources, rather than redistribution.

## CHAPTER 7: CONCLUSION

Our findings directly address key questions relating to the interactions among fire, wind, vegetation, and soil processes in a shrub-grass transition ecosystem using a unique multiple tracer-based approach. We tested the field applicability of a potentially valuable tracer technique, REE tracers for wind erosion studies, which could be used to monitor landscape responses to disturbances and for grassland/habitat management programs. In our study, while fires are seen to dramatically increase sediment transport and nutrient loss, they can also potentially be used in our study environment as a valuable tool to manage shrub-encroached grasslands.

We observed that fire caused a significant decrease of the VWC underneath shrub sites, removed the sheltering effect provided by shrubs, lowered the TSV of both shrub and grass sites (shrub sites have the lowest TSV), and allowed for an increase in the shear velocity of wind at the soil surface. These mechanisms caused a threefold increase in HMF and VDF as well as induced changes in sediment sources and sinks following the fire, overall, leading to a homogenization of surface sediment and nutrients. These processes are thought to enhance grass regrowth by providing a negative feedback mechanism to woody plant encroachment.

In a regime of predicted climatic and land-cover shifts, a potential increase in aridity in drylands may enhance the frequency and intensity of fires, leading to acceleration of soil erosion processes and a prolonged post-fire window of soil erosion disturbances. Considering the extent of grassland and rangelands (70% of the world's drylands) and the multitude of ecosystem services (including primary production and carbon sequestration) they provide, understanding the interactions among vegetation dynamics, disturbance, and

soil erosion is critical. Our study presents the first step towards developing a valuable tool to monitor the ecogeomorphic response of these landscapes to changing climate, disturbance, and management scenarios.

## REFERENCES CITED

- Anderies, J. M., M. A. Janssen, and B. H. Walker (2002), Grazing management, resilience, and the dynamics of a fire-driven rangeland system, *Ecosystems*, 5(1), 23–44.
- Archer, S., D. S. Schimel, and E. A. Holland (1995), Mechanisms of shrubland expansion: Land use, climate or CO<sub>2</sub>?, *Clim. Change*, 29(1), 91–99, doi:10.1007/BF01091640.
- Báez, S., and S. L. Collins (2008), Shrub invasion decreases diversity and alters community stability in northern Chihuahuan desert plant communities, *PLoS One*, 3(6), e2332.
- Bagnold, R. A. (1941), Threshold wind speed and size of sand grain, *The physics of wind blown sand and desert dunes*, pp. 85-94, Methuen, London.
- Bowman, D. M. J. S., J. K. Balch, P. Artaxo, W. J. Bond, J. M. Carlson, M. A. Cochrane, C. M. D’Antonio, R. S. DeFries, J. C. Doyle, and S. P. Harrison (2009), Fire in the Earth system, *Science*, 324(5926), 481–484.
- Breshears, D. D., J. J. Whicker, M. P. Johansen, and J. E. Pinder (2003), Wind and water erosion and transport in semi-arid shrubland, grassland and forest ecosystems: quantifying dominance of horizontal wind-driven transport, *Earth Surf. Process. Landforms*, 28(11), 1189–1209, doi:10.1002/esp.1034.
- Buffington, L. C., and C. H. Herbel (1965), Vegetational Changes on a Semidesert Grassland Range from 1858 to 1963, *Ecol. Monogr.*, 35(2), 139–164, doi:10.2307/1948415.
- Burkhardt, J. (2010), Hygroscopic particles on leaves: nutrients or desiccants?, *Ecol. Monogr.*, 80(3), 369–399.
- Campbell, G. S., J. M. Norman (1998), Wind, *An Introduction to Environmental Biophysics*, 63-75, Springer + Business Media inc., New York.
- Casenave, A., and C. Valentin (1992), A runoff capability classification system based on surface features criteria in semi-arid areas of West Africa, *J. Hydrol.*, 130(1–4), 231–249.
- Chepil, W. S. (1956), Influence of Moisture on Erodibility of Soil by Wind, *Soil Sci. Soc. Am. J.*, 20(2), 288-292, doi:10.2136/sssaj1956.03615995002000020033x.
- Cornelis, W.M. (2006), Hydroclimatology of wind erosion in arid and semi-arid environments, in *Dryland Ecohydrology*, edited by P. D’Odorico and A. Porporato, 141-159, Springer, Dordrecht.

- Cornelis, W. M., D. Gabriels, and R. Hartmann (2004), A conceptual model to predict the deflation threshold shear velocity as affected by near-surface soil water: I. Theory, *Soil Sci. Soc. Am. J.*, 68, 1154-1161, doi:10.2136/sssaj2004.1154.
- D'Odorico, P., A. Bhattachan, K. F. Davis, S. Ravi, and C. W. Runyan (2013), Global desertification: Drivers and feedbacks, *Adv. Water Resour.*, 51, 326–344, doi:10.1016/j.advwatres.2012.01.013.
- D'Odorico, P., F. Laio, and L. Ridolfi (2006), Patterns as indicators of productivity enhancement by facilitation and competition in dryland vegetation, *J. Geophys. Res. Biogeosciences*, 111(G3).
- D'Odorico, P., G. S. Okin, and B. T. Bestelmeyer (2012), A synthetic review of feedbacks and drivers of shrub encroachment in arid grasslands, *Ecohydrology*, 5(5), 520–530.
- Darkoh, M. B. K. (1998), The nature, causes and consequences of desertification in the drylands of Africa, *L. Degrad. Dev.*, 9(1), 1–20, doi:10.1002/(SICI)1099-145X(199801/02)9:1<1::AID-LDR263>3.0.CO;2-8.
- Deasy, C., and J. N. Quinton (2010), Use of rare earth oxides as tracers to identify sediment source areas for agricultural hillslopes, *Solid Earth*, 1(1), 111–118, doi:10.5194/se-1-111-2010.
- DeBano, L. F. (1966), Formation of non-wettable soils: involves heat transfer mechanism, *Pacific Southwest Forest and Range Experiment Station*, vol. 132, 1-8.
- DeBano, L. F. (2000), The role of fire and soil heating on water repellency in wildland environments: a review, *J. Hydrol.*, 231(2000), 195–206.
- Dunne, T., Field studies of hillslope flow processes, *Hillslope Hydrol.*, edited by M. J. Kirkby, pp. 227–293, John Wiley and Sons, Chichester, UK.
- Field, J. P., J. Belnap, D. D. Breshears, J. C. Neff, G. S. Okin, J. J. Whicker, T. H. Painter, S. Ravi, M. C. Reheis, and R. L. Reynolds (2010), The ecology of dust, *Front. Ecol. Environ.*, 8(8), 423–430, doi:10.1890/090050.
- Gibbens, R. P., R. P. McNeely, K. M. Havstad, R. F. Beck, and B. Nolen (2005), Vegetation changes in the Jornada Basin from 1858 to 1998, *J. Arid Environ.*, 61(4), 651–668, doi:10.1016/j.jaridenv.2004.10.001.
- Gillette, D. A., and A. M. Pitchford (2004), Sand flux in the northern Chihuahuan desert, New Mexico, USA, and the influence of mesquite-dominated landscapes, *J. Geophys. Res.*, 109(F4), 1–12, doi:10.1029/2003JF000031.
- Gillette, D. A., and P. H. Stockton (1989), The effect of nonerodible particles on wind erosion of erodible surfaces, *J. Geophys. Res. Atmos.*, 94(D10), 12885–12893.

- Gillette, D. A., D. W. Fryrear, T. E. Gill, T. Ley, T. A. Cahill, and E. A. Gearhart (1997), Relation of vertical flux of particles smaller than 10  $\mu\text{m}$  to total aeolian horizontal mass flux at Owens Lake, *J. Geophys. Res. Atmos.*, *102*(D22), 26009–26015.
- Gromet, L. P., L. A. Haskin, R. L. Korotev, and R. F. Dymek (1984), The “North American shale composite”: its compilation, major and trace element characteristics, *Geochimica et Cosmochimica Acta*, *48*(12), 2469–2482.
- Guzmán, G., J. N. Quinton, M. A. Nearing, L. Mabit, and J. A. Gómez (2013), Sediment tracers in water erosion studies: current approaches and challenges, *J. Soils Sediments*, *13*(4), 816–833, doi:10.1007/s11368-013-0659-5.
- Haines, W. B. (1925), Studies in the physical properties of soils: II. A note on the cohesion developed by capillary forces in an ideal soil, *J. Agric. Sci.*, *15*(4), 529–535.
- Higgins, R. W., Y. Yao, and X. L. Wang (1997), Influence of the North American monsoon system on the US summer precipitation regime, *J. Clim.*, *10*(10), 2600–2622.
- Horton, R. E. (1933), The role of infiltration in the hydrologic cycle, *Eos, Trans. Am. Geophys. Union*, *14*(1), 446–460.
- Huenneke, L. F., J. P. Anderson, M. Remmenga, and W. H. Schlesinger (2002), Desertification alters patterns of aboveground net primary production in Chihuahuan ecosystems, *Glob. Chang. Biol.*, *8*(3), 247–264.
- Huxman, T. E., B. P. Wilcox, D. D. Breshears, R. L. Scott, K. A. Snyder, E. E. Small, K. Hultine, W. T. Pockman, and R. B. Jackson (2005), Ecohydrological Implications of Woody Plant Encroachment, *Ecology*, *86*(2), 308–319.
- Iversen, J. D., and B. R. White (1982), Saltation threshold on Earth, Mars, and Venus, *Sedimentology*, *29*, 111–119, doi:10.1111/j.1365-3091.1982.tb01713.x.
- Johnson, W. R. (1988), Soil survey of Socorro county area, New Mexico. USDA Soil Conservation Service, in cooperation with USDI BLM and BIA, and NM Agricultural Experiment Station. Accessed online: [https://www.nrcs.usda.gov/Internet/FSE\\_MANUSCRIPTS/new\\_mexico/NM664/0/Socorro.pdf](https://www.nrcs.usda.gov/Internet/FSE_MANUSCRIPTS/new_mexico/NM664/0/Socorro.pdf). 13 January 2017
- Kimoto, A., M. A. Nearing, X. C. Zhang, and D. M. Powell (2006), Applicability of rare earth element oxides as a sediment tracer for coarse-textured soils, *Catena*, *65*(3), 214–221, doi:http://dx.doi.org/10.1016/j.catena.2005.10.002.

- Kok, J. F., E. J. R. Parteli, T. I. Michaels, and D. B. Karam (2012), The physics of wind-blown sand and dust, *Reports Prog. Phys.*, 75(10), 106901, doi:10.1088/0034-4885/75/10/106901.
- Krammes, J. S., and L. F. DeBano (1965), Soil wettability: a neglected factor in watershed management, *Water Resour. Res.*, 1(2), 283–286.
- Lal, R. (2001), Soil degradation by water erosion, *L. Degrad. Dev.*, 12(6), 519–539.
- Land, M., B. Öhlander, J. Ingri, and J. Thunberg (1999), Solid speciation and fractionation of rare earth elements in a spodosol profile from northern Sweden as revealed by sequential extraction, *Chem. Geol.*, 160(1), 121–138.
- Larney, F. J., M. S. Bullock, H. H. Janzen, B. H. Ellert, and E. C. S. Olson (1998), Wind erosion effects on nutrient redistribution and soil productivity, *J. Soil Water Conserv.*, 53(2), 133–140.
- Letey, J. (2001), Causes and consequences of fire-induced soil water repellency, *Hydrol. Process.*, 15(15), 2867–2875.
- Li, J., G. S. Okin, L. Alvarez, and H. Epstein (2007), Quantitative effects of vegetation cover on wind erosion and soil nutrient loss in a desert grassland of southern New Mexico, USA, *Biogeochemistry*, 85, 317–332, doi:10.1007/s10533-007-9142-y.
- Li, J., G. S. Okin, L. Alvarez, and H. Epstein (2008), Effects of wind erosion on the spatial heterogeneity of soil nutrients in two desert grassland communities, *Biogeochemistry*, 88(1), 73–88, doi:10.1007/s10533-008-9195-6.
- Li, J., G. S. Okin, and H. E. Epstein (2009), Effects of enhanced wind erosion on surface soil texture and characteristics of windblown sediments, *J. Geophys. Res. Biogeosciences*, 114(G2).
- Li, J., G. S. Okin, J. E. Herrick, J. Belnap, S. M. Munson, and M. E. Miller (2010), A simple method to estimate threshold friction velocity of wind erosion in the field, *Geophys. Res. Lett.*, 37(10), 1–5, doi:10.1029/2010GL043245.
- Markert, B. (1987), The pattern of distribution of lanthanide elements in soils and plants, *Phytochemistry*, 26(12), 3167–3170.
- Marticorena, B., and G. Bergametti (1995), Modeling the atmospheric dust cycle: 1. Design of a soil-derived dust emission scheme, *J. Geophys. Res. Atmospheres*, 100(D8), 16415–16430.
- Millennium Ecosystem Assessment (MEA) (2005), *Ecosystems and human well-being: desertification synthesis*, World Resources Institute. Island Press, Washington, DC.

- Middleton, N., and D. Thomas (1997), *World atlas of desertification*, No. Ed. 2, Arnold, Hodder Headline, PLC.
- Miller, M. E., Bowker, M. A., Reynolds, R. L., Goldstein, H. L. (2012), Postfire land treatments and wind erosion – lessons from the Milford Flat fire, UT, USA. *Aeol. Res.* 7, 29–44.
- Munson, S. M., J. Belnap, G. S. Okin (2011), Responses of wind erosion to climate induced vegetation changes on the Colorado Plateau. *Proc. Nat. Acad. Sci.* 108, 3854–3859.
- Nash, M. S., E. Jackson, and W. G. Whitford (2004), Effects of intense, short-duration grazing on microtopography in a Chihuahuan Desert grassland, *J. Arid Environ.*, 56(3), 383–393.
- NCSS Statistical Software [Computer software], Retrieved from <https://www.ncss.com/download/ncss/updates/ncss-11/>
- Okin, G. S. (2008), A new model for wind erosion in the presence of vegetation, *J. Geophys. Res.*, 113, F02S10, doi:10.1029/2007JF000758.
- Okin, G. S., and D. A. Gillette (2001), Distribution of vegetation in wind-dominated landscapes: Implications for wind erosion modeling and landscape processes, *J. Geophys. Res.*, 106(D9), 9673–9683, doi:10.1029/2001JD900052.
- Okin, G. S., D. A. Gillette, and J. E. Herrick (2006), Multi-scale controls on and consequences of aeolian processes in landscape change in arid and semi-arid environments, *J. Arid Environ.*, 65(2), 253–275, doi:10.1016/j.jaridenv.2005.06.029.
- Parmenter, R. R. (2008), Long-term effects of a summer fire on desert grassland plant demographics in New Mexico, *Rangel. Ecol. Manag.*, 61(2), 156–168.
- Paysen, T. E., R. J. Ansley, J. K. Brown, G. J. Gottfried, S. M. Haase, M. G. Harrington, M. G. Narog, S. S. Sackett, and R. C. Wilson (2000), Fire in western shrubland, woodland, and grassland ecosystems, *USDA For. Serv. Gen. Tech Rep.*, 2, 121–159.
- Polyakov, V. O., and M. A. Nearing (2004), Rare earth element oxides for tracing sediment movement, *Catena*, 55(3), 255–276, doi:10.1016/S0341-8162(03)00159-0.
- Polyakov, V. O., M. A. Nearing, and M. J. Shipitalo (2004), Tracking sediment redistribution in a small watershed: implications for agro-landscape evolution, *Earth Surf. Process. Landforms*, 29(10), 1275–1291, doi:10.1002/esp.1094.
- Ravi, S., T. M. Zobeck, T. M. Over, G. S. Okin, and P. D’Odorico (2006), On the effect of moisture bonding forces in air-dry soils on threshold friction velocity of wind erosion, *Sedimentology*, 53(3), 597–609, doi:10.1111/j.1365-3091.2006.00775.x.

- Ravi, S., P. D'Odorico, T. M. Zobeck, T. M. Over, and S. L. Collins (2007), Feedbacks between fires and wind erosion in heterogeneous arid lands, *J. Geophys. Res.*, *112*(G4), 1–7, doi:10.1029/2007JG000474.
- Ravi, S., P. D'Odorico, L. Wang, C. S. White, G. S. Okin, S. A. Macko, and S. L. Collins (2009a), Post-fire resource redistribution in desert grasslands: A possible negative feedback on land degradation, *Ecosystems*, *12*(3), 434–444, doi:10.1007/s10021-009-9233-9.
- Ravi, S., P. D'Odorico, S. L. Collins, and T. E. Huxman (2009b), Can biological invasion induce desertification?, *New Phytol.*, *181*(3), 512–515, doi: 10.1111/j.1469-8137.2009.02736.x.
- Ravi, S., P. D'Odorico, T. E. Huxman, and S. L. Collins (2010a), Interactions between soil erosion processes and fires: implications for the dynamics of fertility islands, *Rangel. Ecol. Manag.*, *63*(3), 267–274.
- Ravi, S., D. D. Breshears, T. E. Huxman, and P. D'Odorico (2010b), Land degradation in drylands: Interactions among hydrologic-aeolian erosion and vegetation dynamics, *Geomorphology*, *116*(3–4), 236–245, doi:10.1016/j.geomorph.2009.11.023.
- Ravi, S., P. D'Odorico, D. D. Breshears, J. P. Field, A. S. Goudie, T. E. Huxman, J. Li, G. S. Okin, R. J. Swap, A. D. Thomas, S. Van Pelt, J. J. Whicker, and T. M. Zobeck (2011), Aeolian processes and the biosphere, *Rev. Geophys.*, *49*(3), 1–45, doi:10.1029/2010RG000328.
- Ravi, S., M. C. Baddock, T. M. Zobeck, and J. Hartman (2012), Field evidence for differences in post-fire aeolian transport related to vegetation type in semi-arid grasslands, *Aeolian Res.*, *7*, 3–10.
- Retta, A., D. V. Armbrust, L. J. Hagen, and E. L. Skidmore (2000), Leaf and stem area relationships to masses and their height distributions in native grasses, *Agron. J.*, *92*(2), 225–230.
- Sankey, J. B., M. J. Germino, and N. F. Glenn (2009), Aeolian sediment transport following wildfire in sagebrush steppe, *J. Arid Environ.*, *73*(10), 912–919, doi:10.1016/j.jaridenv.2009.03.016.
- Sankey, J. B., N. F. Glenn, M. J. Germino, A. I. N. Gironella, and G. D. Thackray (2010), Relationships of aeolian erosion and deposition with LiDAR-derived landscape surface roughness following wildfire, *Geomorphology*, *119*(1), 135–145.

- Sankey, J. B., M. J. Germino, and N. F. Glenn (2012a), Dust supply varies with sagebrush microsites and time since burning in experimental erosion events, *J. Geophys. Res. Biogeosciences*, 117(G1).
- Sankey, J. B., M. J. Germino, T. T. Sankey, and A. N. Hoover (2012b), Fire effects on the spatial patterning of soil properties in sagebrush steppe, USA: a meta-analysis, *Int. J. Wildl. Fire*, 21(5), 545–556.
- Sankey, J. B., S. Ravi, C. S. A. Wallace, R. H. Webb, and T. E. Huxman (2012c), Quantifying soil surface change in degraded drylands: Shrub encroachment and effects of fire and vegetation removal in a desert grassland, *J. Geophys. Res. Biogeosciences*, 117(G2).
- Sankey, J. B., Law, D., Breshears, D. D., Munson, S. M., Webb, R. H. (2013), Employing LiDAR to detail vegetation canopy architecture for prediction of aeolian transport. *Geophys. Res. Lett.*, 40, doi: 10.1002/grl.50356.
- Schlesinger, W. H., J. F. Reynolds, G. L. Cunningham, L. F. Huenneke, W. M. Jarrell, R. A. Virginia, and W. G. Whitford (1990), Biological feedbacks in global desertification., *Science*, 247(4946), 1043–1048, doi:10.1126/science.247.4946.1043.
- Shao, Y. (2008), *Physics and modelling of wind erosion*, 37, Springer Science & Business Media.
- Shao, Y., M. R. Raupach, and P. A. Findlater (1993), Effect of saltation bombardment on the entrainment of dust by wind, *J. Geophys. Res.*, 98(D7), 12719-12726, doi:10.1029/93JD00396.
- Stockton, P. H., and D. A. Gillette (1990), Field measurement of the sheltering effect of vegetation on erodible land surfaces, *L. Degrad. Dev.*, 2(2), 77–85, doi:10.1002/ldr.3400020202.
- Stout, J. E. (2012), A field study of wind erosion following a grass fire on the Llano Estacado of North America, *J. Arid Environ.*, 82, 165–174.
- Swap, R., M. Garstang, S. A. Macko, P. D. Tyson, W. Maenhaut, P. Artaxo, P. Kallberg, and R. Talbot (1996), The long-range transport of southern African aerosols to the tropical South Atlantic, *J. Geophys. Res.*, 101(19), 777–791.
- Turnbull, L., B. P. Wilcox, J. Belnap, S. Ravi, P. D’Odorico, D. Childers, W. Gwenzi, G. Okin, J. Wainwright, and K. K. Caylor (2012), Understanding the role of ecohydrological feedbacks in ecosystem state change in drylands, *Ecohydrology*, 5(2), 174–183.

- UNCCD (1994), United Nations Convention to Combat Desertification in Countries Experiencing Serious Drought And/or Desertification, Particularly in Africa. A/ AC.241/27., , (September), 1–58, doi:Accessed online: <http://www.unccd.int/convention/menu.php>.
- US EPA (United States Environmental Protection Agency) (2007), SW-846 Test Method 3051A, Revision 1. Microwave assisted acid digestion of sediments, sludges, soils, and oils. United States Environmental Protection Agency, Washington, D.C., <https://www.epa.gov/hw-sw846/sw-846-test-method-3051a-microwave-assisted-acid-digestion-sediments-sludges-soils-and-oils>, accessed 15 January, 2017.
- Van Gosen, B., P. Verplanck, K. Long, J. Gambogi, Joseph, and Seal (2014), The Rare-Earth Elements — Vital to Modern Technologies and Lifestyles, *U.S. Geol. Surv. Fact Sheet 2014–3078*, 4, doi:<http://dx.doi.org/10.3133/fs20143078>.
- Van Pelt, R. S., and T. M. Zobeck (2007), Chemical constituents of fugitive dust, *Environ. Monit. Assess.*, 130(1–3), 3–16.
- Van Pelt, R. S., M. C. Baddock, M. C. W. Barnes, J. E. Strack, and T. M. Zobeck (2012), Use of rare earth elements in investigations of aeolian processes, Control ID=1490034, *Proc. Am. Geophys. Union Fall Meeting*, Dec 3-7, 2012, San Francisco, CA.
- Van Pelt, R. S. et al. (2014), Using rare earth element tracers to investigate aeolian processes, *Proc. Eighth Int. Conf. Aeolian Res.*, pp. 4-5, ICAR XIII, July 21-25, 2014, Lanzhou, China.
- Van Pelt, R. S., M. C. Baddock, T. M. Zobeck, P. D’Odorico, S. Ravi, and A. Bhattachan (2017a), Total vertical sediment flux and PM10 emissions from disturbed Chihuahuan Desert surfaces, *Geoderma*, 293, 19–25, doi:10.1016/j.geoderma.2017.01.031.
- Van Pelt, R.S., M. C. W. Barnes, and J. E. Strack (2017b), Wind-driven dispersion of sediments from a point source: Use of rare earth elements as tracers in aeolian field studies. *Aeolian Res.*, (in review).
- Westoby, M., B. Walker, and I. Noy-Meir (1989), Range management on the basis of a model which does not seek to establish equilibrium, *J. Arid Environ.*, 17(2), 235–239.
- Whicker, J. J., D. D. Breshears, P. T. Wasiolek, T. B. Kirchner, R. A. Tavani, D. A. Schoep, and J. C. Rodgers (2002), Temporal and Spatial Variation of Episodic Wind Erosion in Unburned and Burned Semiarid Shrubland, *J. Environ. Qual.*, 31(2), 599-612, doi:10.2134/jeq2002.0599.

- White, C. S., R. L. Pendleton, and B. K. Pendleton (2006), Response of two semiarid grasslands to a second fire application, *Rangel. Ecol. Manag.*, 59(1), 98–106.
- Wytenbach, A., V. Furrer, P. Schlegli, and L. Tobler (1998), Rare earth elements in soil and in soil-grown plants, *Plant Soil*, 199(2), 267–273.
- Zhang, X. C., J. M. Friedrich, M. A. Nearing, and L. D. Norton (2001), Potential use of Rare Earth Oxides as Tracers for Soil Erosion and Aggregation Studies, *Soil Sci. Soc. Am. J.*, 65(5), 1508-1515, doi:10.2136/sssaj2001.6551508x.
- Zhang, X. C., M. A. Nearing, V. O. Polyakov, and J. M. Friedrich (2003), Using Rare-Earth Oxide Tracers for Studying Soil Erosion Dynamics, *Soil Sci. Soc. Am. J.*, 67(1), 279-288, doi:10.2136/sssaj2003.0279.
- Zhu, M., S. Tan, H. Dang, and Q. Zhang (2011), Rare earth elements tracing the soil erosion processes on slope surface under natural rainfall, *J. Environ. Radioact.*, 102(12), 1078–1084.

**APPENDIX A: DATA**

Windy Season Horizontal Mass Flux (3/11/16 – 6/11/16). .....81

Bare microsite REE concentrations. ....81

Grass site REE concentrations. ....84

Shrub site REE concentrations. ....85

Ho and Eu in burned area microsities. ....86

Burned area normalized REE concentrations. ....87

Burned area normalized sediment collector REE concentrations. ....89

Normalized Spiked REE concentrations. ....89

Control area normalized REE concentrations. ....90

Control area normalized sediment sampler REE concentrations. ....93

For meteorological tower data see  
[https://drive.google.com/open?id=0B\\_hO5MD3vroyend3WWWh2aWlrUWc](https://drive.google.com/open?id=0B_hO5MD3vroyend3WWWh2aWlrUWc)

Windy Season Horizontal Mass Flux (3/11/16 – 6/11/16)	
Horizontal Mass Flux (g / m d)	Treatment area
28.01638638	Control
28.32433466	Control
24.37328963	Control
30.73844964	Control
24.85411294	Control
26.15202414	Control
36.95577876	Burned
43.95773009	Burned
60.30092049	Burned
185.2171049	Burned
56.86133726	Burned
68.35803172	Burned

Bare microsite REE concentrations								
Spike d Yb	Control Yb	Burned Yb	Spiked Eu	Control Eu	Burned Eu	Spike d Ho	Control Ho	Burned Ho
20.933138	14.22056791	6.88262306	0.29321068	2.16048069	1.144539676	0.3022129	0.27690686	0.48903991
13.76305	191.2631953	407.275613	0.23060893	0.28335626	1.13197596	0.264681	0.24080708	1.68971284
104.02686	125.6320334	266.164741	0.25632697	0.31180996	1.642929787	0.4828991	0.19404853	1.22853139
189.68389	6.173968917	338.807152	9.78770315	0.24880512	0.776662486	0.2374721	2.22555629	0.39480391
471.86904	353.0377505	247.681028	0.46385749	0.30275798	0.79347313	0.2810806	3.36162236	0.97016311
234.26307	214.0172161	38.776497	0.45290914	0.37242121	0.845157548	0.2814222	0.14341551	19.0113909
48.195565	83.30625361	192.321741	0.3545713	1.70183926	0.837023884	0.3387473	0.20054264	3.92328339
38.900611	143.0323182	133.240999	0.44069065	0.41763101	3.757663135	0.2892968	0.30336727	5.05056867
156.67888	100.4659439	121.924016	0.25278322	10.6114081	1.22205428	0.3175117	0.33043662	1.16134885
299.18068	43.56043647	426.673749	0.32044476	0.33763338	5.815088505	0.5497301	0.30886301	3.86320938
363.57574	299.4116806	139.716784	0.41512947	0.4020863	1.383680025	8.6313723	0.25320893	0.9286449
166.78074	84.96966567	204.210656	0.36716703	0.35681659	0.451605477	0.4201117	0.30361161	0.41322012

111.55 134	5.96413 7791	178.37 5391	0.4194 3149	0.3649 268	0.87020 9112	0.3410 513	0.3165 7366	0.4968 3015
307.27 862	198.017 2995	243.68 6908	2.4918 1456	0.3717 9532	1.09893 7647	0.3277 416	0.2898 3211	0.5881 7473
35.935 196	327.817 3107	272.31 1021	0.4534 5556	0.3766 0736	0.59156 5711	0.3323 323	0.3080 4952	0.3239 1692
446.24 265	179.713 2893	168.68 1548	0.4349 0187	0.4345 0414	0.78964 8039	0.3265 617	0.2812 8183	0.3826 48
173.17 963	173.406 6856	175.83 4398	0.5764 9539	0.3961 9853	0.46696 9715	0.3001 924	0.3317 4345	0.6109 6637
3.6112 775	68.2717 4032	305.41 4483	0.3287 0142	0.4595 3869	0.59782 2811	0.2822 744	0.2940 646	0.4823 621
132.09 657	330.936 2759	18.544 3516	0.5470 8339	0.4437 3954	0.47263 3924	0.2718 921	0.2899 6315	1.3497 0467
243.78 935	331.682 5799	311.10 4774	2.4616 9953	0.3842 8918	0.69092 0435	0.2710 462	0.2534 9455	1.4491 9138
118.59 303	64.5279 8559	32.859 3815	0.6533 7442	0.4196 2463	1.18625 0526	0.2686 619	0.3402 2056	1.6708 0813
53.533 507	217.446 9988	103.39 2546	0.4037 8739	0.4143 1154	0.60024 7625	0.5985 305	0.2948 3021	0.2996 4729
335.95 996	141.031 6683	159.50 8581	0.8455 205	0.3137 1149	0.65189 4239	0.2416 362	0.2579 4501	0.4625 4888
259.62 208	232.511 3652	216.84 5969	0.3571 8758	0.3706 834	0.49548 9603	0.2590 466	0.2862 3674	0.2643 0863
176.97 429	199.009 4196	226.33 3552	0.3399 0594	1.0046 628	1.92298 3968	0.2813 264	0.2366 368	0.9891 2613
197.87 456	227.013 0487	308.85 2715	0.2719 6076	0.5432 518	0.96418 0171	0.2406 236	0.2443 0252	0.5913 5638
142.98 677	263.209 2172	108.03 5462	0.4816 6763	0.3825 5926	0.90351 1364	0.4548 85	0.2573 6106	0.5033 5486
167.05 672	259.511 0734	13.809 515	0.3979 8194	0.3868 2152	0.91914 7962	0.2740 047	0.3466 8245	7.1514 4554
149.04 957	167.429 3655	7.4774 155	0.4248 0359	0.3718 4569	1.03171 6917	0.2093 148	0.2486 1729	3.2323 2287
126.38 302	376.627 3893	260.26 9022	0.3943 3989	0.4703 7007	0.63182 7229	0.5161 828	0.9332 904	1.0755 3042
181.30 808	241.673 8246	125.17 1103	0.3211 3872	0.4493 2278	0.65527 4711	0.2017 111	0.2411 2807	0.4073 6456
123.78 229	216.770 6919	77.095 0304	0.3656 4501	0.6546 8666	0.39560 4485	0.2785 215	0.2865 598	0.3058 7413
267.72 587	428.870 8073	*	0.3432 0549	1.8712 2537	*	0.3630 068	0.2585 2852	*
342.25 38	466.718 9198	*	0.3430 8515	1.3506 6742	*	0.2333 088	0.2081 9708	*
197.86 261	88.9345 161	*	0.3661 6677	0.4779 7532	*	0.2248 617	0.3065 4123	*

298.91 963	157.918 2198	*	0.4136 2355	3.5363 6533	*	0.1923 257	16.795 2064	*
1276.7 38	140.589 0223	*	0.6318 2723	0.4055 4486	*	0.2381 71	0.3536 6355	*
870.33 58	253.889 9963	*	0.6552 7471	0.4927 535	*	0.4902 616	0.2320 0981	*
828.88 2	239.802 6435	*	0.3956 0449	0.4175 9282	*	0.4991 767	0.3416 1871	*
*	188.707 7014	*	*	0.3957 4585	*	*	0.2753 12	*
*	50.2819 5229	*	*	0.9318 9071	*	*	0.2526 6078	*
*	222.487 898	*	*	0.4725 6656	*	*	0.3136 8043	*
*	584.450 816	*	*	0.7581 5656	*	*	0.2725 346	*
*	270.970 9629	*	*	0.4274 6147	*	*	0.3165 0624	*
*	490.402 0719	*	*	0.4347 131	*	*	0.1686 9525	*
*	247.905 0079	*	*	0.4840 6394	*	*	0.2575 4363	*
*	84.8214 2793	*	*	0.3473 0661	*	*	0.2383 0466	*
*	64.6821 0539	*	*	0.9862 2645	*	*	14.809 4614	*
*	67.2686 2771	*	*	0.5100 3878	*	*	0.2702 2237	*
*	222.824 0601	*	*	0.5077 7097	*	*	0.3801 8696	*
*	132.840 1893	*	*	0.4205 2303	*	*	0.3097 3861	*
*	53.3505 4167	*	*	12.113 0256	*	*	0.1935 8903	*
*	279.611 3358	*	*	0.5375 1424	*	*	0.2678 0018	*
*	68.7661 929	*	*	0.5141 8878	*	*	0.2788 4834	*
*	331.720 5268	*	*	0.6727 1127	*	*	0.4521 8879	*
*	352.747 4092	*	*	0.4569 5264	*	*	0.3242 1928	*
*	377.099 9923	*	*	0.6942 5466	*	*	0.3145 0752	*

Grass site REE concentrations								
Spiked Ho	Control Ho	Burned Ho	Spiked Eu	Control Eu	Burned Eu	Spike d Yb	Control Yb	Burned Yb
0.6708 1147	0.18558 9585	2.96680 1478	24.3194 5643	4.91363 4255	24.742 3337	2.323 9398	3.0066 5095	18.40 0162
0.2344 731	0.30022 0686	0.60059 4299	8.80290 477	4.39936 8191	92.984 3846	1.623 5114	20.692 0991	10.43 4205
0.1596 0069	0.32616 4044	7.65866 4086	71.2123 6372	11.8587 2235	12.988 1252	2.681 3894	11.899 4904	22.89 1607
0.3881 5702	0.24129 023	1.67383 3338	23.4630 4756	6.99652 4053	41.717 8338	1.545 2223	8.1768 7826	6.760 4918
0.2905 9516	0.27581 8778	15.1943 8435	37.6628 0582	4.99384 9633	71.003 6822	1.354 249	11.124 6975	18.04 5291
0.0911 0097	0.26251 4603	1.32171 6996	187.045 5819	101.540 3573	28.770 0141	1.972 6759	15.345 1498	5.678 465
0.1614 091	0.16949 3616	0.30398 3757	236.009 7515	59.9351 9467	55.554 0981	1.672 6659	10.949 776	2.706 5369
0.0396 4273	0.04444 2081	0.37637 6939	175.123 8559	44.0377 4037	53.371 602	2.521 1665	15.158 8689	2.896 5148
*	0.09039 2543	1.20456 2239	*	9.68593 9047	103.44 024	*	4.1008 1535	42.82 4027
*	0.15251 6247	1.50531 0334	*	34.0175 32	41.579 7517	*	3.1664 4666	4.460 227
*	0.25761 0768	1.65787 6178	*	0.90101 0847	58.019 5235	*	3.5328 7675	11.44 3759
*	0.32897 2581	2.91040 0497	*	16.9969 3047	2.3333 2863	*	2.8195 1404	13.78 9326
*	0.16676 5946	2.14114 0294	*	43.7520 5252	247.00 8909	*	5.1426 9425	17.06 3513
*	0.15971 5439	0.35900 8333	*	54.8491 7398	80.443 2946	*	3.9059 8241	3.908 815
*	*	2.17306 9918	*	*	18.743 5585	*	*	45.07 8464

Shrub site REE concentrations								
Spiked Ho	Control Ho	Burned Ho	Spiked Yb	Control Yb	Burned Yb	Spiked Eu	Control Eu	Burned Eu
64.491 35	70.741 93	229.86 19	2.1913 17	3.1064 46	7.7943 01	0.3543 66	0.2748 77	0.9805 14
67.987 04	96.711 23	84.783 42	1.3792 11	1.7951 38	8.9110 36	0.2826 38	0.8384 22	0.8440 25
15.447 64	52.959 18	22.137 13	3.0110 67	1.8986 79	1.6033 79	0.2486 44	0.3858 19	0.3015 19
244.85 53	172.66 98	30.222 25	0.5768 36	5.4797 46	2.2360 21	0.2588 54	0.4226 18	0.4919 17
19.589 72	14.145 41	78.499 03	1.1841 72	3.1064 9	14.947 75	0.2652 57	0.3563 9	1.9714 05
79.962 37	173.61 8	29.103 02	0.7603 98	2.1422 82	1.7923 5	0.2658 07	0.5080 66	0.3410 33
58.170 7	67.118 15	73.780 68	1.6721 42	3.9891 59	3.9866 39	0.2596 36	0.3489 64	0.4135 54
66.069 53	119.74 86	22.270 73	1.1445 6	2.7735 2	3.1184 59	0.3908 41	0.2903	0.4440 36
368.73 19	23.365 34	211.72 51	0.5418 12	0.9194 79	2.9424 81	0.4533 89	0.2913 99	0.9641 94
467.46 51	101.20 04	111.91 09	0.2745 44	1.3786 53	7.3769 37	0.4015 76	0.3851 66	1.1264 79
360.33 04	*	104.47 18	0.9229 17	*	12.717 92	0.3867 2	*	1.5748 63
*	*	30.089 7	*	*	7.6623 96	*	*	0.9012 46
*	*	76.502 34	*	*	4.3840 81	*	*	0.4103 72
*	*	2.0595 17	*	*	0.6350 44	*	*	0.4744
*	*	5.3580 06	*	*	1.4239 68	*	*	0.4163 29
*	*	20.793 47	*	*	0.7975 5	*	*	0.3537 68

Ho and Eu in burned area microsites			
Ho in Grass	Eu in Shrub	Eu in Bare	Ho in Bare
2.966801	0.980514	1.14454	0.48904
0.600594	0.844025	1.131976	1.689713
7.658664	0.301519	1.64293	1.228531
1.673833	0.491917	0.776662	0.394804
15.19438	1.971405	0.793473	0.970163
1.321717	0.341033	0.845158	19.01139
0.303984	0.413554	0.837024	3.923283
0.376377	0.444036	3.757663	5.050569
1.204562	0.964194	1.222054	1.161349
1.50531	1.126479	5.815089	3.863209
1.657876	1.574863	1.38368	0.928645
2.9104	0.901246	0.451605	0.41322
2.14114	0.410372	0.870209	0.49683
0.359008	0.4744	1.098938	0.588175
2.17307	0.416329	0.591566	0.323917
*	0.353768	0.789648	0.382648
*	*	0.46697	0.610966
*	*	0.597823	0.482362
*	*	0.472634	1.349705
*	*	0.69092	1.449191
*	*	1.186251	1.670808
*	*	0.600248	0.299647
*	*	0.651894	0.462549
*	*	0.49549	0.264309
*	*	1.922984	0.989126
*	*	0.96418	0.591356
*	*	0.903511	0.503355
*	*	0.919148	7.151446
*	*	1.031717	3.232323
*	*	0.631827	1.07553
*	*	0.655275	0.407365
*	*	0.395604	0.305874

Burned area normalized REE concentrations					
Microsite Type	Sample Name	La (ppm)	Yb (normalized)	Eu (normalized)	Ho (normalized)
bare	243 Burned Plot 1 Sample 11 PE	9.44706	0.267484	0.006961	0.0024
bare	245 Burned Plot 1 Sample 39 PE	6.944561	0.037998	0.002955	0.047017
bare	123 Burned Plot 2 Sample 1 PE	8.20559	0.133334	0.017581	0.01199
bare	124 Burned Plot 2 Sample 2 PE	7.948344	0.121913	0.004848	0.002232
bare	129 Burned Plot 2 Sample 6 PE	7.746897	0.429474	0.027913	0.009011
bare	131 Burned Plot 2 Sample 8 PE	8.41797	0.13987	0.00566	0.001648
bare	132 Burned Plot 2 Sample 9 PE	8.006069	0.204959	0.000979	0.000355
bare	133 Burned Plot 2 Sample 10 PE	8.118822	0.178885	0.003081	0.000565
bare	135 Burned Plot 2 Sample 12 PE	7.070759	0.244799	0.00423	0.000794
bare	136 Burned Plot 2 Sample 13 PE	7.853524	0.273687	0.001682	0.000131
bare	138 Burned Plot 2 Sample 15 PE	7.080593	0.169102	0.002677	0.000278
bare	217 Burned Plot 2 Sample 24 PE	7.109714	0.032027	0.004668	0.00351
bare	250 Burned Plot 3 Sample 15 PE	6.775704	0.21771	0.001199	0
bare	247 Burned Plot 3 Sample 19 PE	7.163202	0.310566	0.003553	0.000802

bare	230 Burned Plot 3 Sample 34 PE	5.547051	0.006411	0.003892	0.007428
bare	140 Burned Plot 2 Sample 17 PE	7.2169	0.176321	0.001056	0.000851
bare	141 Burned Plot 2 Sample 18 PE	7.781119	0.307096	0.001713	0.000528
bare	142 Burned Plot 2 Sample 19 PE	6.111261	0.01758	0.001085	0.002704
bare	143 Burned Plot 2 Sample 20 PE	7.220643	0.312839	0.002181	0.002954
grass	242 Burned Plot 1 Sample 37 PE	7.232683	0.017434	0.122959	0.006762
grass	244 Burned Plot 1 Sample 45 PE	6.803078	0.009395	0.465649	0.000825
grass	125 Burned Plot 2 Sample 3 PE	6.612422	0.005687	0.208205	0.003518
grass	126 Burned Plot 2 Sample 4 PE	6.543823	0.017076	0.355269	0.03744
grass	127 Burned Plot 2 Sample 5 PE	6.64823	0.021967	0.063933	0.018533
grass	130 Burned Plot 2 Sample 7 PE	6.461599	0.004595	0.143185	0.002634
grass	134 Burned Plot 2 Sample 11 PE	5.532852	0.001596	0.277686	8.07E-05
grass	220 Burned Plot 2 Sample 11 PE	6.396853	0.001787	0.266726	0.000262
grass	137 Burned Plot 2 Sample 14 PE	6.491094	0.042083	0.518155	0.00234
grass	218 Burned Plot 2 Sample 23 PE	7.264851	0.003366	0.207512	0.003095

grass	246 Burned Plot 3 Sample 17 PE	6.733633	0.010413	0.290067	0.003478
grass	248 Burned Plot 3 Sample 49 PE	6.542362	0.012781	0.010428	0.00662
shrub	239 Burned Plot 1 Sample 17 PE	3.769573	0.00673	0.003635	0.576034
shrub	236 Burned Plot 1 Sample 18 PE	5.623752	0.007857	0.00295	0.212037
shrub	235 Burned Plot 1 Sample 19 PE	5.493957	0.000482	0.000225	0.054859
shrub	237 Burned Plot 1 Sample 20 PE	5.747578	0.001121	0.001181	0.075145
shrub	238 Burned Plot 1 Sample 29 PE	5.036146	0.01395	0.008611	0.196269
shrub	241 Burned Plot 1 Sample 50 PE	10.58257	0.024847	0.023506	0.176277
shrub	139 Burned Plot 2 Sample 16 PE	5.976903	0.000673	0.000424	0.072336
shrub	216 Burned Plot 2 Sample 32a PE	5.602791	0.002888	0.000788	0.184431
shrub	219 Burned Plot 2 Sample 32b PE	6.420523	0.002011	0.000941	0.055194
shrub	249 Burned Plot 3 Sample 3 PE	5.810597	0.001834	0.003553	0.530529
shrub	232 Burned Plot 3 Sample 16 PE	5.587261	0.006309	0.004368	0.280099
shrub	233 Burned Plot 3 Sample 39 PE	4.561051	0.011699	0.00662	0.261434
shrub	234 Burned Plot 3 Sample 40 PE	5.298312	0.006597	0.003237	0.074812

shrub	231 Burned Plot 3 Sample 41 PE	4.979857	0.003289	0.000772	0.19126
-------	--------------------------------	----------	----------	----------	---------

Burned area normalized sediment collector REE concentrations				
Sample Name	La	Yb (normalized)	Eu (normalized)	Ho (normalized)
177 Burned Sediment Collector 8	6.186157	0.388901	0.146086	0.18998
178 Burned Sediment Collector 9	5.640015	0.291213	0.147854	0.29111
179 Burned Sediment Collector 10	7.163806	0.192231	0.114318	0.091555
147 Burned Sediment Collector 3	7.32158	0.224393	0.126221	0.211154
161 Burned Sediment Collector 4	6.148218	0.415249	0.173751	0.653664
162 Burned Sediment Collector 5	6.07766	0.274809	0.111796	0.667295
163 Burned Sediment Collector 6	7.064767	0.153904	0.082597	0.341173
164 Burned Sediment Collector 7	7.411304	0.022573	0.008897	0.018441

Normalized Spiked REE concentrations				
Sample Name	La	Yb (normalized)	Eu (normalized)	Ho (normalized)
39 Burned Plot 1 Bare PA	8.58624	1.287379	0.000582	0
42 Burned Plot 2 Bare PA	7.451593	0.877228	0.001361	0.000548
45 Burned Plot 3 Bare PA	6.758612	0.835392	0.00266	0.00057
40 Burned Plot 1 Grass PA	6.486336	0.000855	0.937995	0
43 Burned Plot 2 Grass PA	6.689549	0.000552	1.183877	0
46 Burned Plot 3 Grass PA	6.07979	0.001409	0.878128	0
41 Burned Plot 1 Shrub PA	4.338276	0	0.000988	0.924454
44 Burned Plot 2 Shrub PA	3.751558	0	0.000728	1.172172

47 Burned Plot 3 Shrub PA	4.81803	0	0.000653	0.903375
------------------------------	---------	---	----------	----------

Control area normalized REE concentrations					
Microsite type	Sample Name	La	Yb (normalized)	Eu (normalized)	Ho (normalized)
bare	215 Control Plot 1 Sample 4 PE	6.25719 5	0.191892	0.000134	0
bare	212 Control Plot 1 Sample 5a PE	6.53119 2	0.125655	0.000277	0
bare	214 Control Plot 1 Sample 7 PE	6.40494	0.355158	0.000232	0.007752
bare	223 Control Plot 1 Sample 13 PE	7.2845	0.214856	0.000581	0
bare	221 Control Plot 1 Sample 30 PE	6.80284 5	0.082939	0.007257	0
bare	148 Control Plot 2 Sample 1 PE	8.83252	0.143216	0.000808	7.91E-05
bare	150 Control Plot 2 Sample 3 PE	7.35850 2	0.042826	0.000407	9.29E-05
bare	151 Control Plot 2 Sample 4 PE	7.79837 2	0.301038	0.00073	0
bare	152 Control Plot 2 Sample 5 PE	7.94202	0.084618	0.000503	7.97E-05
bare	153 Control Plot 2 Sample 6 PE	8.80873	0.004883	0.000544	0.000112
bare	155 Control Plot 2 Sample 8 PE	8.36928 4	0.198708	0.000578	4.52E-05
bare	156 Control Plot 2 Sample 9 PE	7.23206	0.329705	0.000602	9.09E-05
bare	158 Control Plot 2 Sample 11 PE	7.93388 4	0.180235	0.000893	2.37E-05
bare	159 Control Plot 2 Sample 12 PE	8.35527 3	0.17387	0.000701	0.00015
bare	165 Control Plot 2 Sample 13 PE	7.14248 4	0.067766	0.001019	5.58E-05
bare	166 Control Plot 2 Sample 14 PE	7.77956 8	0.332853	0.000939	4.55E-05
bare	168 Control Plot 2 Sample 16 PE	6.64999 9	0.333606	0.000641	0
bare	169 Control Plot 2 Sample 17 PE	6.35273 3	0.063987	0.000818	0.000172
bare	171 Control Plot 2 Sample 19 PE	7.69359 4	0.218317	0.000792	5.77E-05

bare	172 Control Plot 2 Sample 20 PE	6.15348 1	0.141197	0.000287	0
bare	175 Control Plot 2 Sample 23 PE	6.81119 6	0.23352	0.000573	3.62E-05
bare	182 Control Plot 2 Sample 24 PE	7.57289 7	0.199709	0.003756	0
bare	183 Control Plot 2 Sample 25 PE	7.67407 8	0.227971	0.001439	0
bare	184 Control Plot 2 Sample 26 PE	7.70229 5	0.264501	0.000632	0
bare	185 Control Plot 2 Sample 27 PE	6.78250 2	0.260769	0.000654	0.000188
bare	186 Control Plot 2 Sample 28 PE	6.58299 5	0.167838	0.000578	0
bare	189 Control Plot 2 Sample 31 PE	7.41818 7	0.378966	0.001073	0.00166
bare	190 Control Plot 2 Sample 32 PE	7.68932	0.242767	0.000968	0
bare	191 Control Plot 2 Sample 33 PE	7.53815 9	0.217634	0.001999	3.7E-05
bare	193 Control Plot 2 Sample 34 PE	7.39601 1	0.431691	0.008108	0
bare	194 Control Plot 2 Sample 35 PE	6.96592 6	0.469888	0.005494	0
bare	195 Control Plot 2 Sample 36 PE	9.02792 8	0.088619	0.001111	8.71E-05
bare	198 Control Plot 2 Sample 39 PE	9.13831 1	0.14075	0.000748	0.000205
bare	200 Control Plot 2 Sample 41 PE	7.63044 7	0.255096	0.001186	0
bare	201 Control Plot 2 Sample 42 PE	9.09945 6	0.240879	0.000808	0.000175
bare	202 Control Plot 2 Sample 43 PE	9.12485	0.189313	0.000698	8.74E-06
bare	204 Control Plot 2 Sample 45 PE	7.94959 4	0.04961	0.003391	0
bare	205 Control Plot 2 Sample 46 PE	8.41004 9	0.223404	0.001084	0.000105
bare	206 Control Plot 2 Sample 47 PE	8.11844 2	0.588706	0.002518	1.77E-06
bare	207 Control Plot 2 Sample 48 PE	8.99100 3	0.272335	0.000858	0.000112
bare	209 Control Plot 2 Sample 49 PE	9.63575 6	0.49379	0.000894	0
bare	210 Control Plot 2 Sample 50 PE	8.64518 5	0.249056	0.001142	0

bare	251 Control Plot 3 Sample 5 PE	7.76197 8	0.084468	0.000455	0
bare	252 Control Plot 3 Sample 16 PE	8.07845 8	0.066753	0.001272	0
grass	149 Control Plot 2 Sample 2 PE	8.49622 5	0.100257	0.051998	0.000147
grass	211 Control Plot 1 Sample 3 PE	6.32060 6	0.013216	0.00956	1.27E-05
grass	222 Control Plot 1 Sample 14 PE	6.79511	0.001899	0.047351	0
grass	154 Control Plot 2 Sample 7 PE	7.94550 6	0.019747	0.023386	7.12E-05
grass	157 Control Plot 2 Sample 10 PE	6.66558 1	0.00238	0.217224	0
grass	167 Control Plot 2 Sample 15 PE	7.05901 2	0.010873	0.020803	0.000136
grass	170 Control Plot 2 Sample 18 PE	5.00640 9	0.007116	0.058262	0
grass	173 Control Plot 2 Sample 21 PE	6.17939 6	0.010091	0.033845	1E-05
grass	174 Control Plot 2 Sample 22 PE	6.10746 9	0.014351	0.023789	0
grass	196 Control Plot 2 Sample 37 PE	7.30209 6	0.009915	0.508615	0
grass	199 Control Plot 2 Sample 40 PE	7.60282 8	0.014163	0.299687	0
grass	203 Control Plot 2 Sample 44 PE	8.21222 6	0.003003	0.219855	0
grass	255 Control Plot 3 Sample 14 PE	6.82757 4	0.00206	0.169536	0
grass	254 Control Plot 3 Sample 38 PE	7.38062 4	0.00243	0.003236	0
shrub	213 Control Plot 1 Sample 5b PE	6.26021 1	0.005095	0	0.004902
shrub	229 Control Plot 3 Sample 8 PE	7.30946 6	0.064143	0.003664	0.036474
shrub	197 Control Plot 2 Sample 38 PE	8.0182	0.158239	0.01647	0.041457
shrub	187 Control Plot 2 Sample 29 PE	5.40772 5	0.001999	9.15E-05	0.176807
shrub	188 Control Plot 2 Sample 30 PE	4.70922 3	0.000676	0.002921	0.241963
shrub	226 Control Plot 3 Sample 9 PE	7.80373 7	0.00078	0.000649	0.132191
shrub	228 Control Plot 3 Sample 17 PE	7.42997 8	0.004394	0.000833	0.432541

shrub	253 Control Plot 3 Sample 20 PE	7.81895 5	0.001999	0.000501	0.034808
shrub	227 Control Plot 3 Sample 30 PE	8.03699 8	0.001026	0.001262	0.43492
shrub	225 Control Plot 3 Sample 39 PE	6.05531 7	0.00289	0.000464	0.167715

Control area normalized sediment sampler REE concentrations				
Sample Name	La	Yb (normalized)	Eu (normalized)	Ho (normalized)
145 Control Sediment Sampler 1	6.768912	0.289051	0.034937	0.00107
146 Control Sediment Sampler 2	7.119543	0.204626	0.025392	0.000912
180 Control Sediment Sampler 11	6.761421	0.096008	0.015047	0.000578
181 Control Sediment Sampler 12	7.297337	0.023315	0.001928	0.000474